Research Article

VX-765 reduces neuroinflammation after spinal cord injury in mice

https://doi.org/10.4103/1673-5374.306096

Date of submission: August 9, 2020

Date of decision: October 7, 2020

Date of acceptance: November 10, 2020

Date of web publication: January 25, 2021

Jing Chen[1, 2, 3, #], Yu-Qing Chen[1, 2, 3, #], Yu-Jiao Shi[1, 2, #], Shu-Qin Ding[1], Lin Shen[2], Rui Wang[2], Qi-Yi Wang[2], Cheng Zha[2], Hai Ding[2], Jian-Guo Hu[1, 2, *], He-Zuo Lü[1, 2, 3, *]

Graphical Abstract *Role of VX-765 on local immune cell subsets and its neuroprotective effect following spinal cord injury (SCI)*

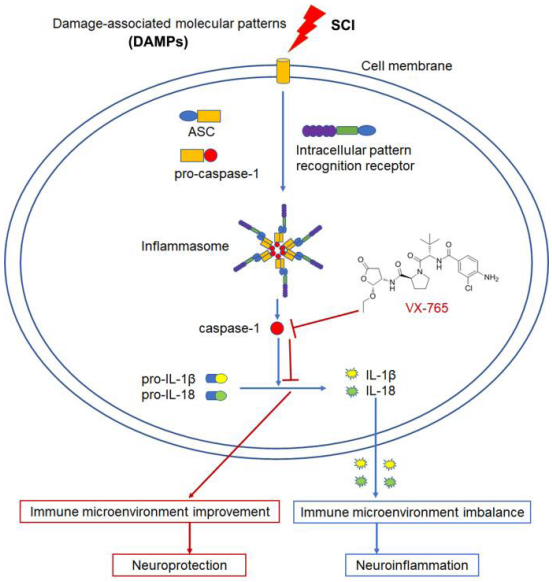

Abstract

Inflammation is a major cause of neuronal injury after spinal cord injury. We hypothesized that inhibiting caspase-1 activation may reduce neuroinflammation after spinal cord injury, thus producing a protective effect in the injured spinal cord. A mouse model of T9 contusive spinal cord injury was established using an Infinite Horizon Impactor, and VX-765, a selective inhibitor of caspase-1, was administered for 7 successive days after spinal cord injury. The results showed that: (1) VX-765 inhibited spinal cord injury-induced caspase-1 activation and interleukin-1β and interleukin-18 secretion. (2) After spinal cord injury, an increase in M1 cells mainly came from local microglia rather than infiltrating macrophages. (3) Pro-inflammatory Th1Th17 cells were predominant in the Th subsets. VX-765 suppressed total macrophage infiltration, M1 macrophages/microglia, Th1 and Th1Th17 subset differentiation, and cytotoxic T cells activation; increased M2 microglia; and promoted Th2 and Treg differentiation. (4) VX-765 reduced the fibrotic area, promoted white matter myelination, alleviated motor neuron injury, and improved functional recovery. These findings suggest that VX-765 can reduce neuroinflammation and improve nerve function recovery after spinal cord injury by inhibiting caspase-1/interleukin-1β/interleukin-18. This may be a potential strategy for treating spinal cord injury. This study was approved by the Animal Care Ethics Committee of Bengbu Medical College (approval No. 2017-037) on February 23, 2017.

Key Words: immune cell subsets; immune function; inflammasomes; leukocyte infiltration; macrophages; microglia; pathways; spinal cord injury

Chinese Library Classification No. R453; R392.3; R744

Introduction

Spinal cord injury (SCI) can be devastating for patients and lacks effective drug treatments (Singh et al., 2014; Rubiano et al., 2015). SCI includes two main pathological processes: primary injury and secondary injury. The former is the direct injury caused by mechanical force, and cannot be predicted or intervened with (Hayta and Elden, 2018). The latter includes local ischemia, edema, electrolyte disorder, lipid peroxidation,

[1]Clinical Laboratory, the First Affiliated Hospital of Bengbu Medical College, Bengbu, Anhui Province, China; [2]Anhui Key Laboratory of Tissue Transplantation, the First Affiliated Hospital of Bengbu Medical College, Bengbu, Anhui Province, China; [3]Department of Immunology, Bengbu Medical College, and Anhui Key Laboratory of Infection and Immunity at Bengbu Medical College, Bengbu, Anhui Province, China

***Correspondence to:** He-Zuo Lü, MD, PhD, lhz233003@163.com; Jian-Guo Hu, MD, PhD, jghu9200@163.com.

https://orcid.org/0000-0002-3889-835X (He-Zuo Lü); https://orcid.org/0000-0002-9055-874X (Jian-Guo Hu)

#These authors contributed equally to this work.

Funding: *The study was supported by the National Natural Science Foundation of China, Nos. 81772321, 82072416 (both to HZL).*

How to cite this article: *Chen J, Chen YQ, Shi YJ, Ding SQ, Shen L, Wang R, Wang QY, Zha C, Ding H, Hu JG, Lü HZ (2021) VX-765 reduces neuroinflammation after spinal cord injury in mice. Neural Regen Res 16(9):1836-1847.*

and inflammation (Popovich, 2014; Ahuja et al., 2017; Rouanet et al., 2017; Hayta and Elden, 2018; Liu et al., 2019a; Chai et al., 2021). Of these, inflammation caused by immune cells is one of the most damaging factors (Rouanet et al., 2017; Ahmed et al., 2018). The inflammatory reaction to SCI includes the activation of local immune cells, the infiltration of peripheral immune cells, and the secretion of proinflammatory cytokines, finally leading to spinal cord dysfunction (Sun et al., 2016). Early and effective anti-inflammatory treatment is therefore important to improve the local immune microenvironment, protect residual neurons, and promote functional recovery. Recently, many basic and clinical studies have been published investigating anti-inflammatory drugs for SCI, such as methylprednisolone (Fehlings et al., 2017), ibuprofen, minocycline (Hayta and Elden, 2018; Aceves et al., 2019), and interleukin (IL)-10 (Thompson et al., 2013; Kitamura et al., 2019). However, only methylprednisolone is currently approved for clinical application in SCI, and it has many unwanted side effects, including wound infection, hyperglycemia, and gastrointestinal bleeding (Karsy and Hawryluk, 2019; Liu et al., 2019b). Therefore, the search for more effective drugs with fewer side effects for the treatment of SCI remains a research hot spot in this field.

Inflammasomes are a kind of high-molecular-weight multi-protein complex, and are mainly composed of intracellular pattern recognition receptors (PRRs), adaptor proteins (namely, apoptosis-associated speck-like protein containing a card [ASC]), and pro-caspase-1 (Martinon et al., 2002; Latz et al., 2013; Jamilloux and Martinon, 2016; Sharma and Kanneganti, 2016; Adornetto et al., 2019; Christgen et al., 2020). When PRRs recognize damage-associated molecular patterns (DAMPs), inflammasomes assemble, which recruit ASC and cause caspase-1 self-cleavage and activation (Martinon et al., 2002; Latz et al., 2013; Jamilloux and Martinon, 2016; Sharma and Kanneganti, 2016; Christgen et al., 2020). Caspase-1, also known as IL-1-converting enzyme, is the key regulator of pro-IL-1β and pro-IL-18 to the active IL-1β and IL-18. This further induces the initial immune cells to differentiate into pro-inflammatory cells, secrete pro-inflammatory cytokines, and induce inflammatory reactions (Martinon et al., 2002; Latz et al., 2013; Jamilloux and Martinon, 2016; Sharma and Kanneganti, 2016; Christgen et al., 2020).

As a key component of the inflammasome, caspase-1 is considered an important target for inhibiting inflammasome activation. Several caspase-1 inhibitors (e.g., VX-740, IDN-6556, and VX-765) have been studied in inflammatory-related diseases (Maroso et al., 2011; Noe et al., 2013; Chen et al., 2018; Flores et al., 2020; Kawahara et al., 2020). Among them, VX-765 (belnacasan), a selective inhibitor of caspase-1 (Wannamaker et al., 2007; Yang et al., 2017), has been demonstrated to be effective in central nervous system diseases (e.g., epilepsy, Alzheimer's disease, and multiple sclerosis) (Maroso et al., 2011; McKenzie et al., 2018; Flores et al., 2020). Notably, VX-765 has reached phase II clinical trials for the treatment of epilepsy (Marchesan et al., 2020). Using RNA sequencing, we recently found that VX-765 application after SCI can inhibit signaling pathways associated with inflammatory responses (Chen et al., 2020a). This suggests that the immune microenvironment of SCI can be improved by inhibiting caspase-1 activation. We therefore hypothesized that VX-765 might ameliorate neuroinflammation and improve functional recovery following SCI. Here, we studied the role of VX-765 on local immune cell subsets and investigated its neuroprotective effects following SCI.

Materials and Methods

Animals

Eight-week-old female C57BL/6 mice (specific-pathogen-free level, weight 18–20 g, *n* = 84) were purchased from Changzhou Cavens Laboratory Animal Ltd. (Changzhou, China; license No. SCXK (Su) 2016-0010). The complete experimental protocol is shown in a flow chart (**Figure 1**). All experiments were designed and reported according to the Animal Research: Reporting of *In Vivo* Experiments (ARRIVE) guidelines. The animal surgery protocol and postoperative care were approved by the Animal Care Ethics Committee of Bengbu Medical College (approval No. 2017-037) on February 23, 2017.

Contusive SCI model establishment and drug administration

The animals were randomly divided into the SCI (*n* = 56) and sham (*n* = 28) groups. Establishment of the contusive SCI model was performed using an Infinite Horizon Impactor (Precision Systems & Instrumentation, Lexington, KY, USA) (Horiuchi et al., 2015; Wu et al., 2016). Briefly, all mice (*n* = 84) were first anesthetized by intraperitoneal injection with 80 mg/kg ketamine and 10 mg/kg xylazine (Sigma-Aldrich, St. Louis, MO, USA). The T7 and T11 spinous processes were then clamped, fixing the spine, and the T9 lamina was excised. A rod (1.3 mm in diameter) was used to produce a moderate contusive SCI model with a force of 50 kdynes. Mice in the sham group received a laminectomy only, without contusion. After the operation, mice were placed into a chamber at 20–22°C and 30–70% humidity. To prevent infections, the mice were administered 50 mg/kg chloramphenicol (Sangon Biotech, Shanghai, China) daily. Artificial bladder emptying was performed three times per day until spontaneous bladder emptying was re-established. The SCI mice were randomly divided into the dimethyl sulfoxide (DMSO; SCI + DMSO, *n* = 28) and VX-765 (SCI + VX-765, *n* = 28) groups. DMSO (100 µL) or VX-765 (MedKoo Biosciences, Inc., Morrisville, NC, USA, 100 mg/kg prepared in DMSO) was intraperitoneally injected immediately after injury and continued once daily for 7 days. The selection of this dose was based on a previous report (Wannamaker et al., 2007).

Western blot assay

At 3 days post-injury (dpi), mice (*n* = 6 per group) were euthanized with 80 mg/kg ketamine (Sigma-Aldrich) and 10 mg/kg xylazine (Sigma-Aldrich), and then perfused with 10 mL phosphate-buffered saline (PBS; 0.01 M, pH 7.4, 4°C). After perfusion, 5 mm segments of spinal cord containing the injury epicenter (or the same spinal cord segments for the sham group) were removed. For western blot assays, the total protein was extracted and analyzed as previously described (Lin et al., 2018). Briefly, the protein extract was obtained using radioimmunoprecipitation assay lysis buffer (Cat# P0013B; Biosharp, Guangzhou, China). Quantitative analysis of the protein concentration was determined using a Bicinchoninic Acid Protein Assay Kit (Cat# P0012; Beyotime, Shanghai, China). For western blot assays, protein supernatants were diluted in sodium dodecyl sulphate-polyacrylamide gel electrophoresis sample loading buffer (Cat# P0015; Beyotime) and boiled for 5 minutes. Next, 40 mg protein was added to each well and electrophoresed in 10% sodium dodecyl sulphate-polyacrylamide gels before being transferred to polyvinylidene difluoride membranes (Cat# SEQ15150; Millipore, Bedford, MA, USA). To block the membranes, 5% (w/v) non-fat dry milk (Cat# P0016; Beyotime) was used at room temperature for 1 hour. The membranes were then incubated with primary antibodies at 4°C overnight. The primary antibodies were as follows: rabbit polyclonal anti-mouse ASC (1:1000; Cat# abx013852; Abbexa, Cambridge, UK), rabbit monoclonal anti-mouse caspase-1 (1:1000; Cat# ab179515; Abcam, Cambridge, MA, USA), rabbit polyclonal anti-mouse β-actin (1:2000; Cat# BL005B; Biosharp), rabbit polyclonal anti-mouse IL-18 (1:2000; Cat# PA5-79481; Invitrogen, Carlsbad, CA, USA), rabbit polyclonal anti-mouse IL-1β (1:2000; Cat# ab9722; Abcam). Next, the membranes were incubated for 1 hour at room temperature

with goat anti-rabbit IgG/horseradish peroxidase secondary antibody (1:10,000; Cat# BL003A; Biosharp). Finally, the immunoreactive target proteins were detected using an enhanced chemiluminescence kit (Cat# 35055; Pierce™, Thermo Fisher Scientific, Waltham, MA, USA) and observed using a Gel-Pro Analyzer (Media Cybernetics, Silver Spring, MD, USA). The optical density values of specific bands were analyzed.

Immunofluorescence double-staining

At 7 dpi, mice (n = 6 per group) were euthanized with 80 mg/kg ketamine and 10 mg/kg xylazine and perfused with PBS, as described in the western blot protocol. The mice were then perfused with 20 mL paraformaldehyde (4%, prepared in PBS) at 4°C. After perfusion, 5 mm segments of spinal cord containing the injury epicenter (or the same spinal cord segments for the sham group) were removed. The spinal cords were then postfixed overnight in 4% paraformaldehyde before being transferred to 30% sucrose (in PBS) at 4°C overnight. Next, the spinal cords were embedded in optimal cutting temperature medium (Tissue-Tek, Sakura Finetek USA Inc., Torrance, CA, USA) and cut into 6 µm transverse sections using a cryostat (CM1900; Leica Microsystems, Bannockburn, IL, USA). For the immunofluorescence assay, slides were incubated with primary antibodies overnight at 4°C. The following day, after being rinsed three times with PBS, the sections were incubated with secondary antibodies at 37°C for 1 hour. **Additional Table 1** shows the details of the primary and secondary antibodies. Finally, the slides were washed three times, coverslipped with medium containing blue nuclear dye (Hoechst 33342; Cat# B2261; Sigma-Aldrich), and examined under a ZEISS Axio observation microscope (Carl Zeiss AG; Jena, Germany). For cell quantification, six mice were used per group. For each animal, cells were counted from five complete cross-sections containing the injury epicenter (0 mm), from rostral (1 and 0.5 mm) to caudal (–1 and –0.5 mm), as previously described (Wu et al., 2018).

Flow cytometry

At 7 dpi, mice (n = 6 per group) were euthanized with 80 mg/kg ketamine and 10 mg/kg xylazine and perfused with PBS. After perfusion, 5 mm segments of spinal cord containing the injury epicenter (or the same spinal cord segments for the sham group) were obtained. The spinal cords were then dissociated into a single-cell suspension. Percoll gradient centrifugation was used to isolate the mononuclear cells as previously described (Chen et al., 2020b). The immune cell subtypes were stained with antibodies from Invitrogen. **Additional Table 2** shows the details of all antibodies. After incubation with the antibodies for 30 minutes at 4°C, the cells were washed with PBS, fixed with 1% paraformaldehyde, and detected using a BD Accuri flow cytometer (BD Bioscience, San Jose, CA, USA). Non-specific staining was controlled using isotype-matched antibodies. The data were analyzed using FlowJo 7.6.1 software (FlowJo, LLC, Ashland, OR, USA).

Histological analyses

At 42 dpi, the remaining animals were euthanized with 80 mg/kg ketamine and 10 mg/kg xylazine and the spinal cords were harvested. Next, 5 µm transverse sections (n = 6 per group) were cut as described in the immunofluorescence protocol. The fibrotic area, residual ventral horn motoneurons, and myelinated white matter were then identified using hematoxylin-eosin (Cat# C0105M; Beyotime), Nissl staining (Cat# C0117; Beyotime), and Luxol fast blue (Cat# L0294; Sigma-Aldrich), respectively, as previously described (Chen et al., 2020b). Images were taken using a ZEISS Axio observation microscope. The fibrotic area measurements and cell quantifications were performed in an unbiased stereological manner using ImageJ software (National Institutes of Health, Bethesda, MD, USA) (Karimi-Abdolrezaee et al., 2006). In the hematoxylin-eosin-stained sections, the fibrotic area was notably darker than the other areas. Fibrosis was quantified by the ratio of the fibrotic area to the intact spinal cord area. For Nissl staining, the existence of Nissl substance and euchromatic nuclei were used to identify surviving ventral horn neurons (Teng et al., 1998). The surviving ventral horn neurons were quantified by counting all such cells from the ventral horn. For Luxol fast blue staining, Image-Pro Plus 5.1 (Media Cybernetics, Inc., Rockville, MD, USA) was used to quantify the myelinated white matter (Chen et al., 2020b). The myelinated white matter was quantified by the ratio of the Luxol fast blue-positive area to the intact spinal cord area. For the three histological analyses, nine complete cross-sections containing the injury epicenter (0 mm), from rostral (1.5, 1, 0.5, and 0.25 mm) to caudal (–1.5, –1, –0.5, and –0.25 mm), were analyzed per animal as previously described (Chen et al., 2020b).

Basso Mouse Scale

The Basso Mouse Scale, a 10-point scale (0–9) system (Basso et al., 2006), was used to assess locomotion after SCI. The scores were evaluated at 1, 3, 7, 14, 21, 28, 35, and 42 dpi. The evaluation was performed by two blinded scorers, while the mice (n = 10 per group) walked freely on an open-field surface for 4 minutes. A score of 9 indicates normal motor function, while 0 indicates complete paralysis. Thus, a higher score indicates better motor function.

Statistical analysis

The repeated measures two-way analysis of variance followed by Bonferroni's *post hoc* analysis was used for all histological and behavioral data. The non-parametric Kruskal-Wallis analysis of variance followed by individual Mann-Whitney U tests was used to analyze all other data. $P < 0.05$ was considered statistically significant. The data were analyzed using SPSS software v.14.0 (SPSS Inc., Chicago, IL, USA).

Results

VX-765 inhibits SCI-induced expression and activation of caspase-1 and its related molecules

The effects of VX-765 on the SCI-induced expression and activation of caspase-1 and its related molecules were analyzed by western blot. As shown in **Figure 2A** and **B**, the 45 and 42 kDa pro-caspase-1 levels were not significantly different among all groups. However, compared with the sham group, the activated 12 and 10 kDa caspase-1 levels were significantly higher in both the DMSO and VX-765 groups (both $P < 0.01$, n = 6), and the 12 and 10 kDa caspase-1 levels were significantly lower in the VX-765 group than in the DMSO group ($P < 0.05$, n = 6). The 32 kDa pro-IL-1β and 17 kDa IL-1β levels were significantly higher in the DMSO group compared with the other two groups ($P < 0.05$ or 0.01, n = 6); in contrast, IL-1β levels were not significantly different between the sham and VX-765 groups ($P > 0.05$, n = 6; **Figure 2C** and **D**). Compared with the other two groups, the pro-IL-18 (24 kDa) and IL-18 (18 kDa and 12 kDa) levels were significantly higher in the DMSO group ($P < 0.05$, n = 6), while there were no differences between the sham and VX-765 groups ($P > 0.05$, n = 6; **Figure 2E** and **F**). **Figure 2G** and **H** show that the levels of 17 and 12 kDa caspase-3, which are related to apoptosis (Porter and Jänicke, 1999), were not significantly different among the groups ($P > 0.05$, n = 6). However, the 31 kDa pro-caspase-3 was significantly higher in the DMSO group compared with the other two groups ($P < 0.1$ or 0.05, n = 6), while there was no difference between the sham and VX-765 groups ($P > 0.05$, n = 6). Compared with the sham group, the 55 and 48 kDa tumor necrosis factor receptor type 1 levels were significantly higher in the DMSO and VX-765 groups (both $P < 0.01$, n = 6), and they were significantly lower in the VX-765 group compared with the DMSO group ($P < 0.05$, n = 6; **Figure 2I** and **J**). There was no significant difference between

the VX-765 and sham groups in 20 kDa IL-6 levels ($P > 0.05$, $n = 6$), but levels were significantly higher in the DMSO group than in the other two groups (both $P < 0.05$, $n = 6$; **Figure 2K** and **L**).

VX-765 inhibits SCI-induced differentiation of macrophages and microglia into M1 cells and increases the differentiation of microglia into M2 cells

CD68, CD45, and CD11b were used to investigate microglia and infiltrated macrophages using immunofluorescence. $CD45^+$ cells are peripheral leukocytes (Thomas, 1989; Hermiston et al., 2003), $CD68^+$ cells are activated macrophages and microglia (Greaves and Gordon, 2002; Chen et al., 2015), and $CD11b^+$ cells are macrophages and microglia (Martin et al., 2017). Therefore, $CD45^+CD11b^+$ cells are peripheral macrophages, while $CD68^+CD11b^+$ cells are activated macrophages and microglia. Our immunofluorescence results revealed that, in the sham-operated spinal cord, $CD68^+$ cells (**Figure 3A**) were very rare. After SCI, there were significantly more $CD68^+$ cells compared with the sham group ($P < 0.01$, $n = 6$; **Figure 3B–D**). The number of $CD68^+$ cells in the VX-765 group (**Figure 3C**) was significantly lower compared with the DMSO (**Figure 3B**) group ($P < 0.05$, $n = 6$; **Figure 3D**). In the sham-operated spinal cord, $CD45^+$ cells (**Figure 3E**) were also very rare. After SCI, there were significantly more $CD45^+$ cells compared with the sham group ($P < 0.01$, $n = 6$; **Figure 3F**, **G**, and **H**). The numbers of $CD45^+$ peripheral leukocytes were not significantly different between the DMSO (**Figure 3F**) and VX-765 (**Figure 3G**) groups ($P > 0.05$, $n = 6$; **Figure 3H**). In the sham-operated spinal cord, typical resting microglia, characterized by many tiny processes, were observed (**Figure 3A** and **E**). After SCI, these cells were activated, with a round or oval morphology (**Figure 3B**, **C**, **F**, and **G**). The numbers of $CD11b^+$ cells were also significantly higher in the DMSO and VX-765 groups compared with the sham group ($P < 0.01$, $n = 6$; **Figure 3I**). Furthermore, the numbers of $CD11b^+$ cells were significantly lower in the VX-765 group (**Figure 3C** and **G**) compared with the DMSO (**Figure 3B** and **F**) group ($P < 0.05$, $n = 6$; **Figure 3I**). Although $CD68^+CD11b^+$ activated macrophages and microglia (**Figure 3A**) and $CD45^+CD11b^+$ peripheral macrophages (**Figure 3E**) were not detected in the sham group, both cell types increased significantly in the DMSO and VX-765 groups (both $P < 0.01$, $n = 6$; **Figure 3B**, **F**, **J**, and **K**). Compared with the DMSO group (**Figure 3B** and **F**), the numbers of $CD68^+CD11b^+$ and $CD45^+CD11b^+$ cells were significantly lower in the VX-765 (**Figure 3C** and **G**) group (both $P < 0.05$, $n = 6$; **Figure 3J** and **K**).

Microglia and infiltrated macrophages were further detected by flow cytometry using CD45, CD11b, and CD68 antibodies (**Figure 4**). In this experiment, $CD45^{high}$ cells were defined as peripheral infiltrated leukocytes, because activated microglia might have low CD45 expression (Sedgwick et al., 1998; Fu et al., 2009). Therefore, $CD68^+CD11b^+$, $CD45^{high}CD11b^+$, $CD45^{-/low}CD11b^+$, $CD45^{high}CD68^+$, $CD45^{-/low}CD68^+$, and $CD45^{high}CD68^-CD11b^-$ cells were defined as activated macrophages and/or microglia, peripheral-derived macrophages, microglia, activated peripheral-derived macrophages, activated microglia, and peripheral-derived leukocytes excluding macrophages, respectively (**Figure 4A**). The statistical results (**Figure 4B**) revealed that, compared with the sham group, the levels of cell subsets (except $CD45^{-/low}CD11b^+$ microglia) in the DMSO group were significantly higher ($P < 0.01$, $n = 6$). In the VX-765 group, the levels of all cell subsets were significantly lower than in the DMSO group ($P < 0.01$ or 0.05, $n = 6$).

To determine the effects of VX-765 on M1 and M2, which are markers of activated microglia and/or macrophages (CD68), specific markers for M1 (C-C chemokine receptor type 7; CCR7) and M2 (arginase-1; ARG1) (Chen et al., 2015) were detected by immunofluorescence. **Figure 5** shows that both $CD68^+CCR7^+$ M1 cells (**Figure 5A**) and $CD68^+Arg1^+$ M2 cells (**Figure 5B**) were very rare in the sham group. In contrast, after SCI (**Figure 5C–F**), both $CD68^+CCR7^+$ M1 cells (**Figure 5C** and **E**) and $CD68^+Arg1^+$ M2 cells (**Figure 5D** and **F**) were significantly increased (both $P < 0.01$, $n = 6$; **Figure 5G** and **H**). The $CD68^+CCR7^+$ M1 cell numbers were significantly lower ($P < 0.01$, $n = 6$; **Figure 5C**, **E**, and **G**), while the $CD68^+Arg1^+$ M2 cell numbers were significantly higher, in the VX-765 group compared with the DMSO group ($P < 0.01$, $n = 6$; **Figure 5D**, **F**, and **H**).

Flow cytometry was also used to analyze M1 and M2 in the injured spinal cords. Here, $CD11b^+CD68^+CCR7^+$ and $CD11b^+CD68^+CCR7^-$ cells were defined as M1 and M2 cells, respectively. In addition, $CD45^{-/low}CD11b^+CD68^+CCR7^+$ and $CD45^{-/low}CD11b^+CD68^+CCR7^-$ cells were defined as microglia-derived M1 and M2 cells, respectively. Moreover, $CD45^{high}CD11b^+CD68^+CCR7^+$ and $CD45^{high}CD11b^+CD68^+CCR7^-$ cells were defined as peripheral infiltrating M1 and M2 cells, respectively (Thomas, 1989; Chen et al., 2015; Martin et al., 2017) (**Figure 6A**). **Figure 6B** shows that the proportions of total M1, peripheral infiltrating M1, and microglia-derived M1 cells were significantly higher after SCI compared with the sham group (all $P < 0.01$, $n = 6$). After VX-765 treatment, their proportions were significantly lower compared with the DMSO group ($P < 0.01$ or 0.05, $n = 6$). In contrast, the total proportions of M2 and microglia-derived M2 cells were significantly lower after SCI compared with the sham group (both $P < 0.01$, $n = 6$). After VX-765 treatment, their proportions were significantly higher compared with the DMSO group (both $P < 0.01$, $n = 6$).

VX-765 inhibits SCI-induced differentiation of T helper (Th)1Th17 cells and promotes Th2 cell differentiation

To determine the effects of VX-765 on Th1, Th2, and Th17 cell subsets, immunofluorescence was used to detect a general marker (CD4) of Th cells, as well as Th1-specific T box transcription factor, GATA-binding protein 3, and retinoid-related orphan nuclear receptor γ-t as markers of Th1, Th2, and Th17 cells (Zhang et al., 2014; Hu et al., 2016b), respectively. As shown in **Figure 7**, all of the Th subsets were very rare in sham-operated spinal cords (**Figure 7A–C**). After injury, they were significantly higher compared with the sham group (all $P < 0.01$, $n = 6$; **Figure 7D–L**). After VX-765 treatment, Th1 cell numbers were significantly lower ($P < 0.05$, $n = 6$; **Figure 7G** and **J**) and Th2 cell numbers were significantly higher ($P < 0.01$, $n = 6$; **Figure 7H** and **K**) compared with the DMSO group (**Figure 7D** and **E**). There were no differences in Th17 cell numbers between these two SCI groups ($P > 0.05$, $n = 6$; **Figure 7F**, **I**, and **L**).

When the Th cell subsets were analyzed using flow cytometry, $CD3^+CD4^+CD183^+CD196^-$ cells, $CD3^+CD4^+CD183^+CD196^+$ cells, $CD3^+CD4^+CD183^-CD196^+$ cells, and $CD3^+CD4^+CD183^-CD196^-$ cells were defined as Th1, Th1Th17, Th17, and Th2 cells, respectively (Chen et al., 2020b) (**Figure 8A**). All Th subsets were significantly higher after SCI compared with the sham group (all $P < 0.01$, $n = 6$; **Figure 8B**). However, the Th1Th17 subset was predominant, and its proportion was significantly lower in the VX-765 group compared with the DMSO group ($P < 0.01$, $n = 6$). In contrast, compared with the DMSO group, the other Th subsets were significantly higher in the VX-765 group ($P < 0.01$ or 0.05, $n = 6$).

VX-765 increases the proportion of regulatory T cells (Tregs) in the injured spinal cord

To further clarify the effects of VX-765 on Tregs, $CD4^+FoxP3^+$ cells in immunofluorescence were defined as Tregs (Miyara et al., 2009). There were very few Tregs in the sham group (**Figure 9A**), and there were also few Tregs following SCI (**Figure 9B** and **C**). The statistical results (**Figure 9D**) revealed that, although the number of Tregs was significantly higher after

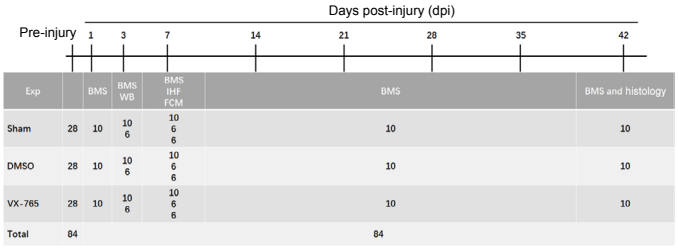

Figure 1 | The complete experimental protocol schedule.
BMS: Basso Mouse Scale; DMSO: dimethyl sulfoxide; Exp: experiment; IHF: immunofluorescence; SCI: spinal cord injury; VX-765: caspase-1 selective inhibitor; WB: western blot.

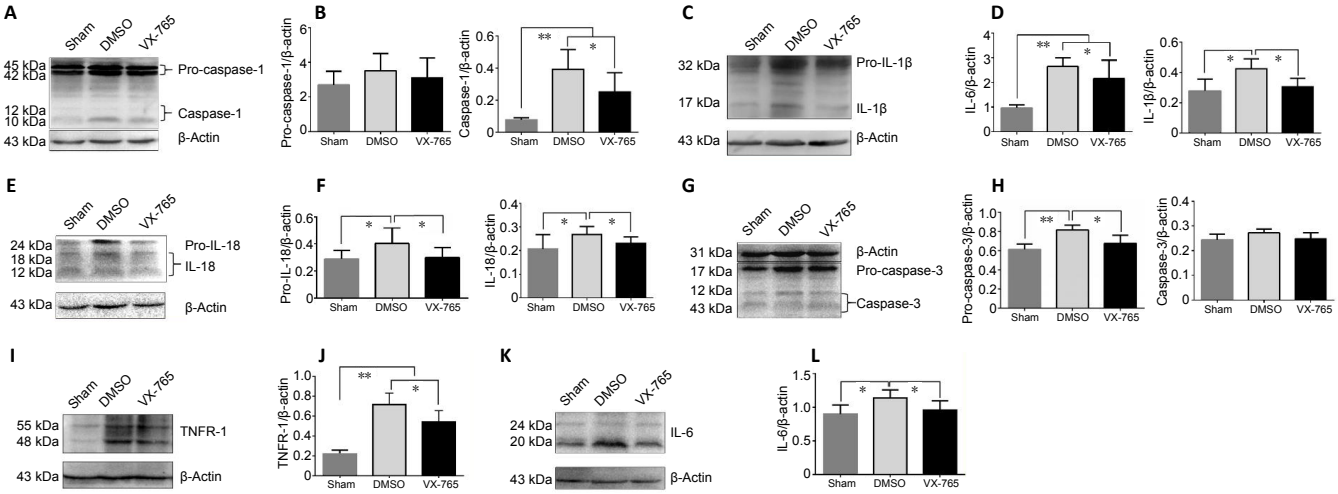

Figure 2 | VX-765 inhibits SCI-induced expression and activities of caspase-1 and related molecules at 3 days post-injury.
(A, C, E, G, I, K) The bands of pro-caspase-1 (45/42 kDa) and cleaved-caspase-1 (10 and 12 kDa) (A), pro-IL-1β (32 kDa) and IL-1β (17 kDa) (C), pro-IL-18 (24 kDa) and IL-18 (18 and 12 kDa) (E), pro-caspase-3 (31 kDa) and caspase-3 (17 and 12 kDa; related to apoptosis) (G), TNFR-1 (55 and 48 kDa) (I), IL-6 (24 and 20 kDa) (K), and β-actin (43 kDa). (B, D, F, H, J, L) Quantitative results of the expression of caspase-1 and related molecules. The original data for Figure 2B, D, F, H, J, and L are shown in Additional file 2. Data are represented as the mean ± SD (n = 6). *P < 0.05, **P < 0.01 (non-parametric Kruskal-Wallis analysis of variance). IL: Interleukin; SCI: spinal cord injury; TNFR-1: tumor necrosis factor receptor type 1; VX-765: caspase-1 selective inhibitor.

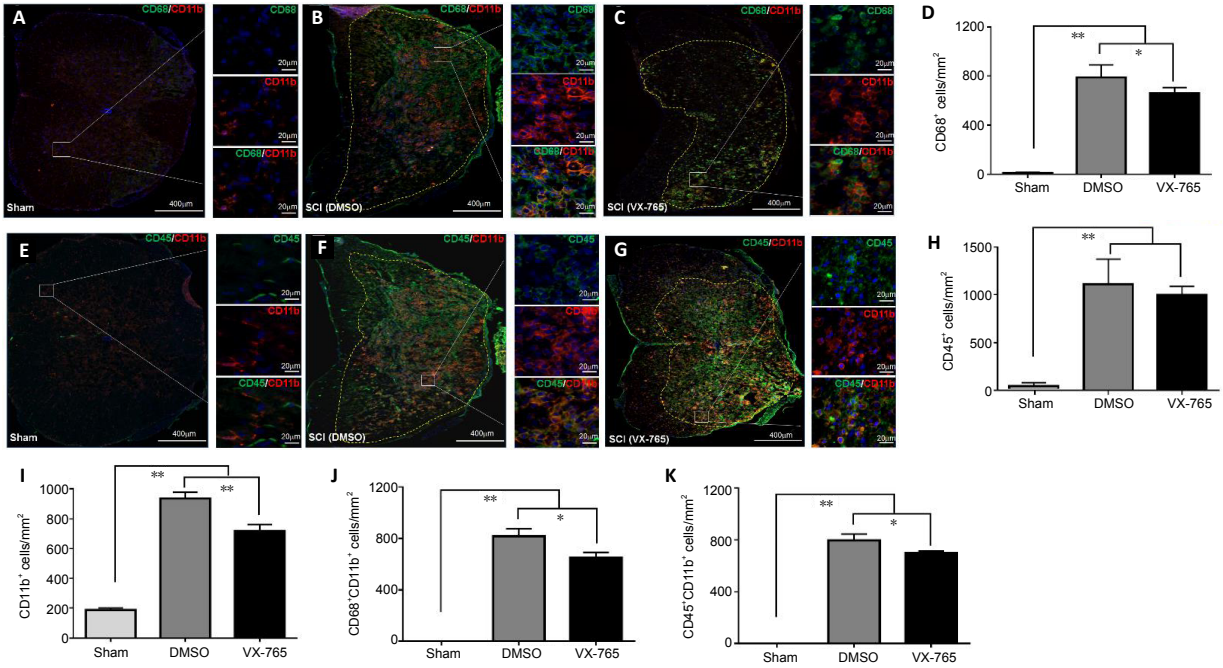

Figure 3 | Effects of VX-765 on microglia and infiltrated macrophages in the injured spinal cord at 7 days post-injury: immunofluorescence detection.
(A–C) CD11b (red, stained by rhodamine) for macrophages and/or microglia, CD68 (green, stained by FITC) for activated macrophages and/or microglia. Nuclei are blue, stained by Hoechst 33342. (D) Quantitative results of $CD68^+$ activated macrophages and/or microglia. (E–G) CD11b (red, stained by rhodamine) for macrophages and/or microglia, CD45 (green, stained by FITC) for peripheral leukocytes. Nuclei are blue, stained by Hoechst 33342. (H–K) Quantitative results of $CD45^+$ peripheral leukocytes (H), $CD11b^+$ macrophages and/or microglia (I), $CD68^+CD11b^+$ activated macrophages and/or microglia (J), and $CD45^+CD11b^+$ macrophages from peripheral blood (K). The original data for Figure 3D, H–K are shown in Additional file 3. Data are represented as the mean ± SD (n = 6). *P < 0.05, **P < 0.01 (non-parametric Kruskal-Wallis analysis of variance). DMSO: Dimethyl sulfoxide; FITC: fluoresceine isothiocyanate; SCI: spinal cord injury; VX-765: caspase-1 selective inhibitor.

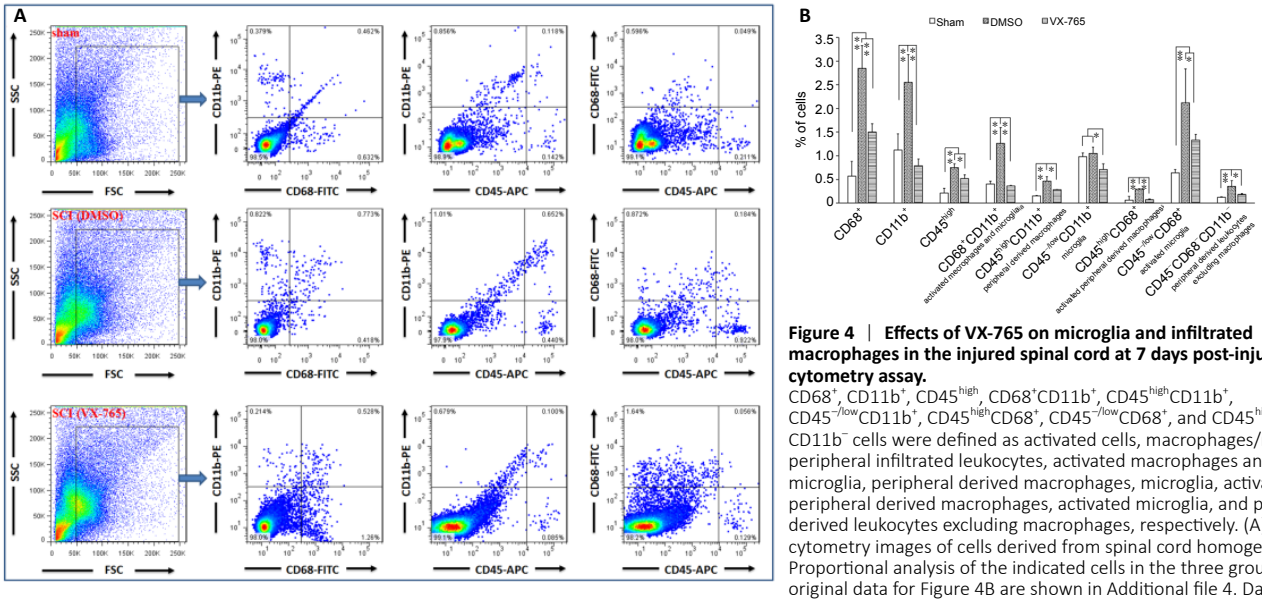

Figure 4 | Effects of VX-765 on microglia and infiltrated macrophages in the injured spinal cord at 7 days post-injury: flow cytometry assay.
$CD68^+$, $CD11b^+$, $CD45^{high}$, $CD68^+CD11b^+$, $CD45^{high}CD11b^+$, $CD45^{-/low}CD11b^+$, $CD45^{high}CD68^+$, $CD45^{-/low}CD68^+$, and $CD45^{high}CD68^-CD11b^-$ cells were defined as activated cells, macrophages/microglia, peripheral infiltrated leukocytes, activated macrophages and/or microglia, peripheral derived macrophages, microglia, activated peripheral derived macrophages, activated microglia, and peripheral-derived leukocytes excluding macrophages, respectively. (A) Flow cytometry images of cells derived from spinal cord homogenate. (B) Proportional analysis of the indicated cells in the three groups. The original data for Figure 4B are shown in Additional file 4. Data are represented as the mean ± SD (n = 6). *P < 0.05, **P < 0.01 (non-parametric Kruskal-Wallis analysis of variance). DMSO: Dimethyl sulfoxide; SCI: spinal cord injury; VX-765: caspase-1 selective inhibitor.

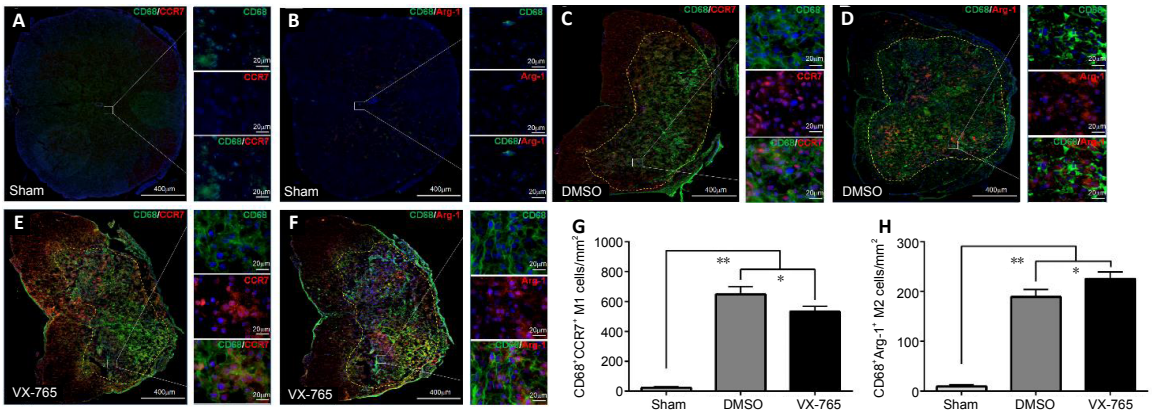

Figure 5 | Effects of VX-765 on M1 and M2 cells in the injured spinal cord at 7 days post-injury: immunofluorescence detection.
(A–F) CD68 (green, stained by FITC) and CCR7 (red, stained by rhodamine) (A, C, and E) for M1 cells, or Arg1 (B, D, and F) for M2 cells, in the different groups. Nuclei are blue, stained by Hoechst 33342. Scale bars: 400 µm, 20 µm (enlarged parts). (G, H) $CD68^+CCR7^+$ M1 (G) and $CD68^+Arg1^+$ M2 (H) cell counts in the sham, DMSO, and VX-765 groups. The original data for Figure 5G and H are shown in Additional file 5. Data are represented as the mean ± SD (n = 6). *P < 0.05, **P < 0.01 (non-parametric Kruskal-Wallis analysis of variance). Arg1: Arginase-1; DMSO: dimethyl sulfoxide; FITC: fluoresceine isothiocyanate; SCI: spinal cord injury; VX-765: caspase-1 selective inhibitor.

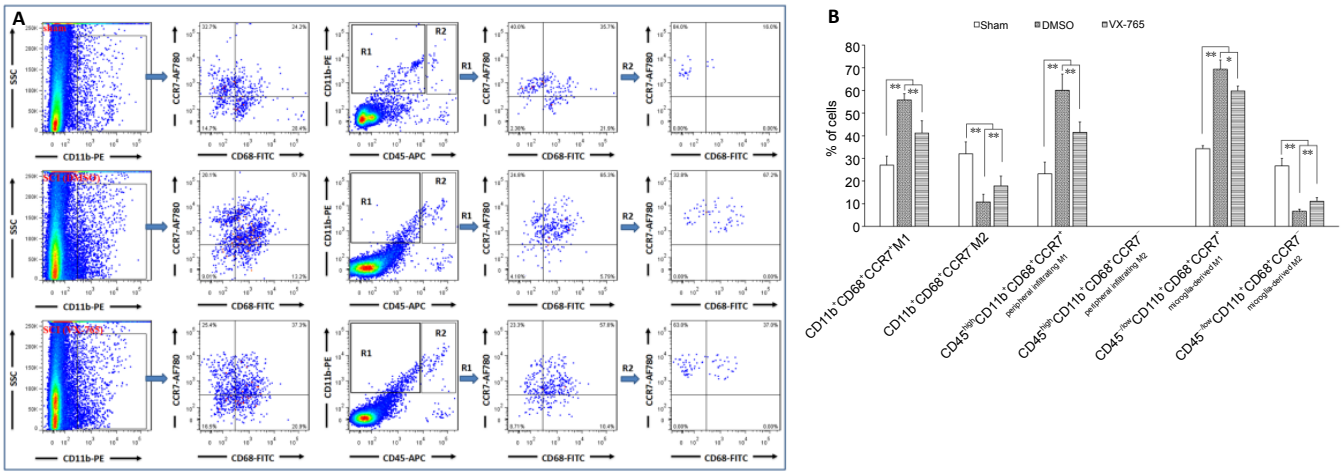

Figure 6 | Effects of VX-765 on M1 and M2 in the injured spinal cord at 7 days post-injury: flow cytometry assay.
$CD11b^+CD68^+CCR7^+$ and $CD11b^+CD68^+CCR7^-$ cells were defined as M1 and M2, respectively. $CD45^{-/low}CD11b^+CD68^+CCR7^+$ and $CD45^{-/low}CD11b^+CD68^+CCR7^-$ cells were defined as microglia-derived M1 and M2, respectively. $CD45^{high}CD11b^+CD68^+CCR7^+$ and $CD45^{high}CD11b^+CD68^+CCR7^-$ cells were defined as peripheral infiltrating M1 and M2, respectively. (A) Flow cytometry images of cells derived from spinal cord homogenate. (B) Proportional analysis of the indicated cells in the sham, DMSO, and VX-765 groups. The original data for Figure 6B are shown in Additional file 6. Data are represented as the mean ± SD (n = 6). *P < 0.05, **P < 0.01 (non-parametric Kruskal-Wallis analysis of variance). DMSO: Dimethyl sulfoxide; SCI: spinal cord injury; VX-765: caspase-1 selective inhibitor.

SCI (all $P < 0.01$, $n = 6$) compared with the sham group, there was no significant difference between the two SCI groups ($P > 0.05$, $n = 6$). For flow cytometry, the $CD3^+CD4^+CD25^+CD127^-$ cell subset was defined as Tregs (Yu et al., 2012) (**Figure 9E**). **Figure 9F** shows that, compared with the sham group, the proportions of Tregs in the DMSO and VX-765 groups were significantly higher (both $P < 0.01$, $n = 6$). After VX-765 treatment, the proportion of Tregs was also significantly higher compared with the DMSO group ($P < 0.01$, $n = 6$).

VX-765 decreases the number of cytotoxic T (Tc) cells in the injured spinal cord

To further clarify the effects of VX-765 on Tc cells, $CD8^+CD28^+$ cells in immunofluorescence were defined as Tc cells (Wu et al., 2017). There were very few Tc cells in the sham group (**Figure 10A**), and a larger number of Tc cells following SCI (**Figure 10B** and **C**). The statistical results (**Figure 10D**) revealed that, compared with the sham group, the numbers of Tc cells in the DMSO and VX-765 groups were significantly higher (both $P < 0.01$, $n = 6$). Compared with the DMSO group, the numbers of Tc cells were significantly lower in the VX-765 group ($P < 0.05$, $n = 6$). $CD3^+CD8^+CD28^+$ cells were also detected using flow cytometry, as previously described (Wu et al., 2017) (**Figure 10E**). **Figure 10F** shows that the proportions of Tc cells in the DMSO and VX-765 groups were significantly higher compared with the sham group (both $P < 0.01$, $n = 6$); however, there was no significant difference between the DMSO and VX-765 groups ($P > 0.05$, $n = 6$).

VX-765 reduces spinal cord tissue damage and promotes functional recovery after SCI

The effects of VX-765 on histology and behavior after SCI were detected at 42 dpi. Representative hematoxylin-eosin and Luxol fast blue images of injured centers are shown in **Figure 11A** and **B**, respectively. In hematoxylin-eosin-stained sections (**Figure 11A**), the butterfly-shaped gray matter was intact and clearly demarcated from the white matter in the sham group. After SCI, the boundary between the gray and white matter was unclear, and the color of the fibrotic area was notably darker than other areas. For Luxol fast blue staining, blue represents the myelinated areas (**Figure 11B**). The statistical results revealed that the effects of VX-765 in fibrotic areas (**Figure 11C**) and spared white matter tissue (**Figure 11D**) could be observed within the range of 0.5 mm (compared with the DMSO group, $P < 0.01$ or 0.05, $n = 10$). The fibrotic area of the VX-765 group was smaller than that of the DMSO group, whereas the myelinated area of the VX-765 group was larger than that of the DMSO group. **Figure 11E** shows images of Nissl staining. The existence of Nissl substance and euchromatic nuclei were used to identify the surviving ventral horn neurons. Significant differences were detected in an area within 1 mm away from the epicenter at the rostral and caudal spinal cords (**Figure 11F**). The VX-765 group had more residual ventral horn motoneurons than the DMSO group ($P < 0.01$ or 0.05, $n = 10$).

To investigate behavioral recovery, the Basso Mouse Scale was used. **Figure 11G** shows that all animals scored 9 points before the operation. After the operation, the sham group still scored 9 points. In contrast, at 1–3 dpi, the scores of the DMSO and VX-765 groups were less than 2 points. From 1–14 dpi, there were no significant differences between the DMSO and VX-765 groups. However, compared with the DMSO group, the Basso Mouse Scale scores of the VX-765 group were significantly higher after 21 dpi ($P < 0.05$, $n = 10$).

Discussion

Previous studies have shown that caspase-1 activation occurs in the injured spinal cord (Mortezaee et al., 2018). VX-765, a compound with a molecular weight of 509 Da and formula of C24H33ClN4O6, reportedly inhibits caspase-1 by inhibiting pro-caspase-1 self-cleavage (Stack et al., 2005; Wannamaker et al., 2007; Zhang and Zheng, 2016; Flores et al., 2018). It has been demonstrated to be effective in central nervous system diseases (Maroso et al., 2011; McKenzie et al., 2018; Flores et al., 2020), collagen-induced arthritis (Zhang and Zheng, 2016), infantile spasms (Galanopoulou et al., 2017), asthma (Chen et al., 2019), atherosclerosis (Li et al., 2020), and some other inflammatory diseases in murine models (Stack et al., 2005). Recently, using RNA sequencing, we also found that VX-765 application following SCI can inhibit signaling pathways associated with inflammatory responses (Chen et al., 2020a). We therefore hypothesized that VX-765 may be an effective anti-inflammatory and neuroprotective drug for treating SCI.

Our western blot results revealed no significant differences in pro-caspase-1 levels between all of the groups. However, the 42–45 kDa bands were at the saturation level. This is because the amount of proteins that were needed per well to detect the activated 12 and 10 kDa cleaved-caspase-1 exceeded the linear phase of detection. However, although the 45 and 42 kDa pro-caspase-1 levels were not found to differ significantly between the groups, western blot analysis confirmed that SCI can induce the activation of caspase-1, IL-1β, and IL-18. These are all involved in the inflammasome-related signaling pathway, and the expression of apoptosis-related molecules (such as pro-caspase-3 and tumor necrosis factor receptor type 1) (Porter and Jänicke, 1999; Idriss and Naismith, 2000) and necrosis-related molecules (such as IL-6) is then induced (Rose-John, 2018). In addition, our findings were consistent with those of previous reports (Wannamaker et al., 2007; Yang et al., 2017). However, we noted that VX-765 decreased pro-caspase-3 levels without affecting the level of activation of caspase-3. This may be because the drug works at the level of gene transcription or translation, although the detailed mechanisms need to be further explored. Nevertheless, our results indicate that VX-765 can indeed inhibit apoptosis- and necrosis-related molecular events, suggesting that VX-765 may be a potential therapeutic drug for SCI. Immediate administration of VX-765 may inhibit inflammation and apoptosis- and necrosis-related molecular events in the injured spinal cord. Thus, we next explored the effects of VX-765 on the immune microenvironment and neuroprotection following SCI.

After SCI, there is destruction of the blood-spinal cord barrier and infiltration of peripheral inflammatory cells, resulting in many immune cell subsets with different functions in the injured spinal cord (Ahmed et al., 2018). Previous studies have reported that infiltrated monocytes and T lymphocytes, and locally activated microglia, play important roles in the pathophysiology of SCI (Hu et al., 2012; Popovich, 2014; Chen et al., 2015; Ma et al., 2015; Hu et al., 2016a; Wu et al., 2017). It has also been confirmed that inflammation is most serious in the subacute stage (1–2 weeks) of SCI (Chen et al., 2015; Wu et al., 2017). We therefore investigated changes in the numbers and proportions of local immune cell subsets at 7 dpi to explore the effects of VX-765 on the local immune microenvironment.

To determine the effects of VX-765 on immune cell subsets, immunofluorescence and flow cytometry were used. The combination of these two methods can not only count the numbers and proportions of immune cell subsets, but can also effectively distinguish peripheral-infiltrated and locally activated cell subsets. They thus provide reliable evidence to understand the effects of VX-765 on the local immune microenvironment in SCI. Our results demonstrated that increased M1 cells were mainly the result of transformation of local microglia, rather than infiltrated macrophages, following SCI in mice. This result suggests that inhibition of local microglia activation after SCI is an important strategy to control the inflammatory response. We also found that an interesting proinflammatory Th1Th17 cell subset (a special

Th subset producing both Th1 and Th17 cytokines) was predominant in the Th subsets of the injured spinal cord. Th1Th17 has a stronger proinflammatory effect than Th1 or Th17 cells (Gosselin et al., 2010; Nikitina et al., 2018). We therefore speculate that Th1Th17 may be another important target for improving the local immune microenvironment in SCI.

In addition, we found the relevance of a 1–3% change in the percentages of immune cells in the pathophysiology generated after SCI. This is because flow cytometry was used to analyze the proportions of immune cells out of all spinal cord cells. Although the proportions were limited, there was a significant imbalance between immune cell subsets, and destructive cells (such as M1, Th1, Th1Th17, and Tc) were predominant after SCI. Our results also showed that VX-765 was able to effectively change this immune imbalance at the injury site. This finding is consistent with a recent report using a stroke model (Li et al., 2019).

The present study also produced some interesting and even seemingly contradictory results, which need further discussion. For example, M2 expression markers were upregulated after SCI in immunofluorescence, but using flow cytometry, the expression of $CD11b^{+}CD68^{+}CCR7^{-}$ indicated a reduction in M2 cells after SCI. Another way of considering this result is that the level of M2 cells in immunofluorescence was extremely low, while the level of M2 using flow cytometry was high. This is likely a technical issue, because immunofluorescence detects the number of cells, whereas flow cytometry measures the proportion of cells. Similarly, using immunofluorescence, Th1 and Th17 levels were lower or remained the same in terms of positive cell numbers, respectively, with VX-765 treatment (relative to injured controls). However, the proportions of markers for Th1 or Th17 were higher with the drug treatment (relative to injured controls) when flow cytometry technology was used. Moreover, there was no significant difference in Treg numbers between the injured groups using immunofluorescence, but with flow cytometry we found a significant increase in Tregs proportion in the VX-765-treated group relative to injured controls. Furthermore, the results related to Tc cells showed a similar situation. Nevertheless, our results indicated that VX-765 was able to suppress the infiltration of total macrophages, the differentiation of M1 macrophages/microglia, the differentiation of Th1 and Th1Th17, and the activation of cytotoxic T cells. Accordingly, this drug may promote the differentiation of M2 microglia, Th2, and Tregs. Our results therefore demonstrate that VX-765 is an immunomodulatory drug for SCI. Next, the effects of VX-765 on histology and behavior following SCI were further explored.

We demonstrated that treatment with VX-765 for 7 consecutive days reduced the fibrotic area, increased white matter myelination and residual motoneurons, and improved functional recovery. Here, the effects of the drug on lesion volume and spared white matter was only observed within a range of approximately 0.5 mm. One reason for this finding may be that VX-765 mainly inhibits the inflammatory response, and the 0.5 mm range contains the area of the most serious immune response. Another reason may be that VX-765 lacks a target for the injured spinal cord. Therefore, understanding the mechanisms of VX-765 in the injured area and exploring a targeted drug delivery system may improve the efficacy of VX-765. Another puzzling finding was that, although the drug was administered for 7 consecutive days, the first signs of behavioral improvement were observed at 21 dpi, which remained for 6 weeks. The likely reason for this phenomenon is that behavioral improvement is based on improvements in histology, and histological improvement is based on improvements in the immune microenvironment at 7 dpi. The observed lag in behavioral improvement can therefore be explained as such.

At present, many drugs or cytokine inhibitors to treat the inflammatory reaction in SCI are in the experimental phase; however, the mechanisms and extent of such treatments are unclear. Moreover, some drugs are effective in experimental SCI models, but not in humans. Currently, steroids are the best clinical drugs for use in early clinical therapy. Therefore, although VX-765 has been demonstrated here to be beneficial in the treatment of SCI, this drug remains in the primary research stage using a mouse model. There are still many underlying mechanisms that need to be explored. For example, we do not know about the drug's turn-over in rodents, or its half-life. It therefore remains to be explored whether continuous administration of VX-765 over 7 days is the best option. In addition, it is unclear how the drug delivery scheme might be optimized and made suitable for humans. One limitation of the present study is that we explored an anti-inflammatory strategy for SCI from the perspective of improving the local immune microenvironment only, even though the pathological mechanisms of SCI are complex. In addition to the inflammatory/immune mechanisms, other factors (such as vascular mechanisms, excitatory amino acid toxicity, peroxide pressure, and astrocyte reactions) are involved in the pathological process of SCI. It may therefore be impossible to rely on a single drug alone, and the development of a comprehensive and feasible treatment plan in this field is urgently needed.

In summary, our results confirm that DAMPs produced by SCI can bind to intracellular PRRs in cells of the injured spinal cord, leading to the assembly of intracellular PRRs, ASC, and pro-caspase-1. This forms the activated inflammasome complex, which causes pro-caspase-1 cleavage and activation. The activated caspase-1 can further cleave pro-IL-1β and pro-IL-18 to form mature IL-1β and IL-18, and results in a local immune microenvironment imbalance, producing neuroinflammation. The use of VX-765 can selectively inhibit the activation of caspase-1, thus inhibiting the production of IL-1β and IL-18, which can improve the local immune microenvironment and produce a neuroprotective effect. The early administration of VX-765 is therefore a promising strategy for the treatment of SCI. However, some limitations remain for the clinical application of VX-765. Our future studies will focus on further clarifying the detailed mechanisms and characteristics of the drug (such as its half-life and side effects), and optimizing the administration scheme.

Author contributions: *Literature search, data interpretation and manuscript writing: HZL; study design: HZL, JGH; data collection: JGH; experiment implementation: JC, YQC, YJS, SQD, LS, CZ; data analysis and figure production: RW, HD, QYW. All authors read and approved the final manuscript.*
Conflicts of interest: *The authors declare that they have no conflict of interests.*
Financial support: *The study was supported by the National Natural Science Foundation of China, Nos. 81772321, 82072416 (both to HZL). The funders had no roles in the study design, conduction of experiment, data collection and analysis, decision to publish, or preparation of the manuscript.*
Institutional review board statement: *The study was approved by the Animal Care Ethics Committee of Bengbu Medical College (approval No. 2017-037) on February 23, 2017.*

Data sharing statement: *Datasets analyzed during the current study are available from the corresponding author on reasonable request.*
Plagiarism check: *Checked twice by iThenticate.*
Peer review: *Externally peer reviewed.*

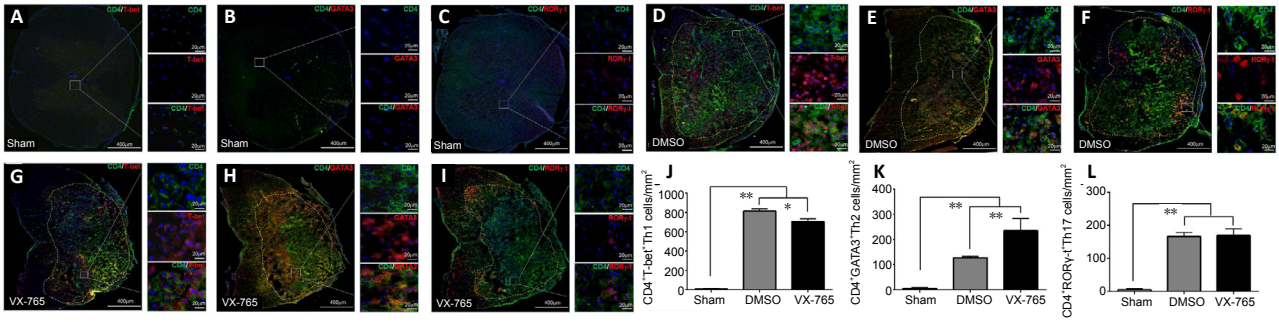

Figure 7 | Effects of VX-765 on Th1, Th2, and Th17 in the injured spinal cord at 7 days post-injury: immunofluorescence detection.
(A–I) CD4 (green, stained by FITC) and T-bet (red, stained by rhodamine) (A, D, and G) for Th1 cells, or GATA3 (red, stained by rhodamine) (B, E, and H) for Th2 cells, or RORγ-t (red, stained by rhodamine) (C, F, and I) for Th17 cells, in the different groups. Nuclei are blue, stained by Hoechst 33342. Scale bars: 400 μm, 20 μm (enlarged parts). (J–L) $CD4^+T\text{-}bet^+$ Th1 (J), $CD4^+GATA3^+$ Th2 (K), and $CD4^+ROR\gamma\text{-}t^+$ Th17 (L) cell counts in the sham, DMSO, and VX-765 groups. The original data for Figure 7J–L are shown in Additional file 7. Data are represented as the mean ± SD (n = 6). *P < 0.05, **P < 0.01 (non-parametric Kruskal–Wallis analysis of variance). DMSO: Dimethyl sulfoxide; FITC: fluoresceine isothiocyanate; GATA3: GATA-binding protein 3; SCI: spinal cord injury; RORγ-t: retinoid-related orphan nuclear receptor γ-t; T-bet: Th1-specific T box transcription factor; Th: T helper; VX-765: caspase-1 selective inhibitor.

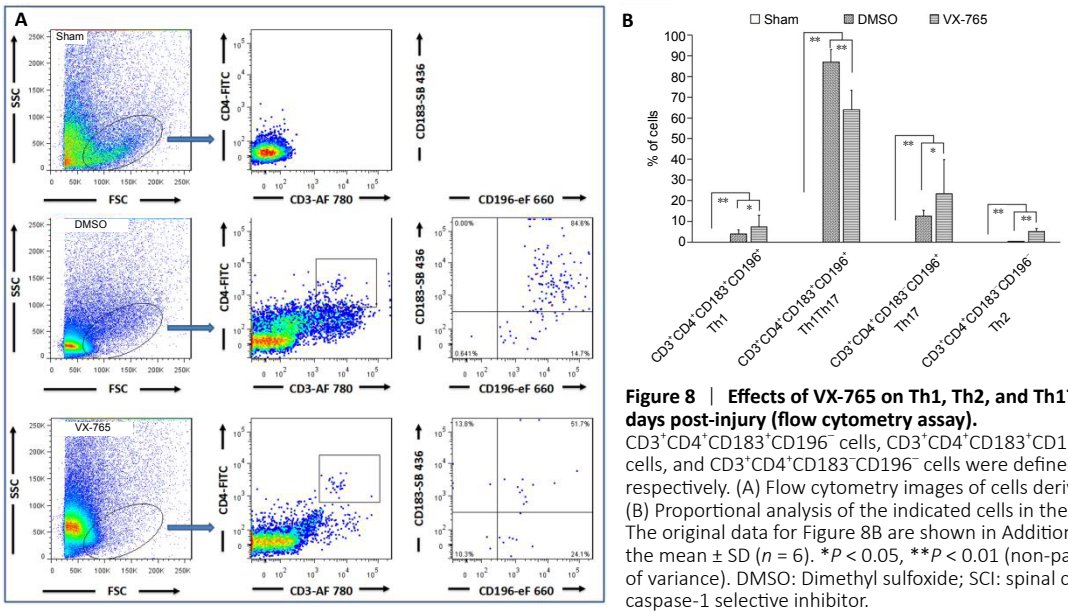

Figure 8 | Effects of VX-765 on Th1, Th2, and Th17 in the injured spinal cord at 7 days post-injury (flow cytometry assay).
$CD3^+CD4^+CD183^+CD196^-$ cells, $CD3^+CD4^+CD183^+CD196^+$ cells, $CD3^+CD4^+CD183^-CD196^+$ cells, and $CD3^+CD4^+CD183^-CD196^-$ cells were defined as Th1, Th1Th17, Th17, and Th2, respectively. (A) Flow cytometry images of cells derived from spinal cord homogenate. (B) Proportional analysis of the indicated cells in the sham, DMSO, and VX-765 groups. The original data for Figure 8B are shown in Additional file 8. Data are represented as the mean ± SD (n = 6). *P < 0.05, **P < 0.01 (non-parametric Kruskal-Wallis analysis of variance). DMSO: Dimethyl sulfoxide; SCI: spinal cord injury; Th: T helper; VX-765: caspase-1 selective inhibitor.

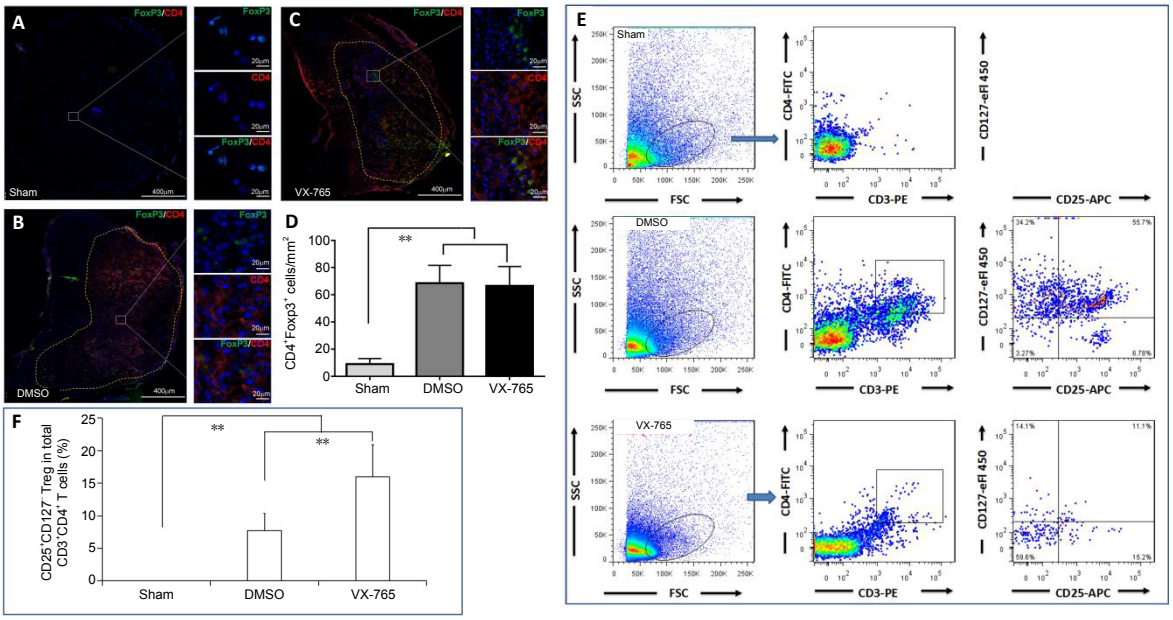

Figure 9 | Effects of VX-765 on Treg in the injured spinal cord at 7 days post-injury: immunofluorescence and flow cytometry assay.
(A–C) CD4 (red, stained by rhodamine) and FoxP3 (green, stained by FITC) for Treg. Nuclei are blue, stained by Hoechst 33342. Scale bars: 400 μm, 20 μm (enlarged parts). (D) $CD4^+FoxP3^+$ Treg cell counts in the sham, DMSO, and VX-765 groups. (E) Flow cytometry images of cells derived from spinal cord homogenate in the different groups. (F) Proportional analysis of $CD3^+CD4^+CD25^+CD127^-$ Treg. The original data for Figure 9D and F are shown in Additional file 9. Data are represented as the mean ± SD (n = 6). **P < 0.01 (non-parametric Kruskal-Wallis analysis of variance). DMSO: Dimethyl sulfoxide; FITC: fluoresceine isothiocyanate; FoxP3: forkhead box P3; SCI: spinal cord injury; Treg: regulatory T cells; VX-765: caspase-1 selective inhibitor.

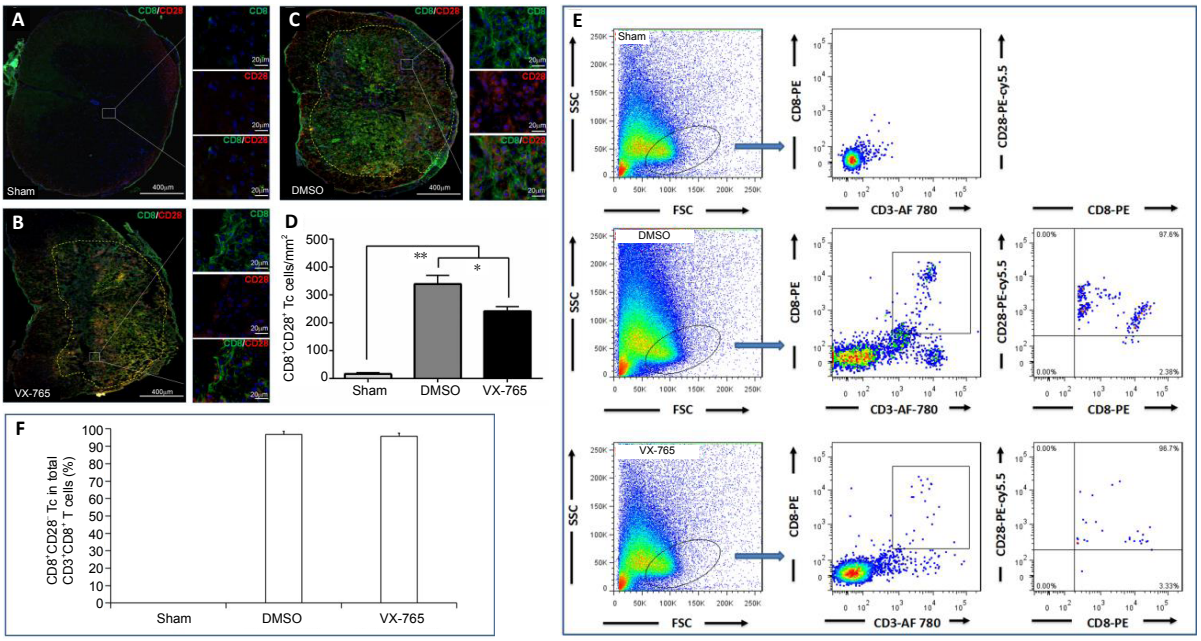

Figure 10 | Effects of VX-765 on Tc cells in the injured spinal cord at 7 days post-injury: immunofluorescence and flow cytometry assay.
(A–C) CD8 (green, stained by FITC) and CD28 (red, stained by rhodamine) for Tc cells in the different groups. Nuclei are blue, stained by Hoechst 33342. (D) $CD8^+CD28^+$ Tc cell counts in the sham, DMSO, and VX-765 groups. (E) Flow cytometry images of cells derived from spinal cord homogenate. (F) Proportional analysis of $CD8^+CD28^+$ Tc cells in the three groups. The original data for Figure 10D and F are shown in Additional file 10. Data are represented as the mean ± SD (n = 6). *P < 0.05, **P < 0.01 (non-parametric Kruskal-Wallis analysis of variance). DMSO: Dimethyl sulfoxide; FITC: fluoresceine isothiocyanate; SCI: spinal cord injury; Tc: cytotoxic T; VX-765: caspase-1 selective inhibitor.

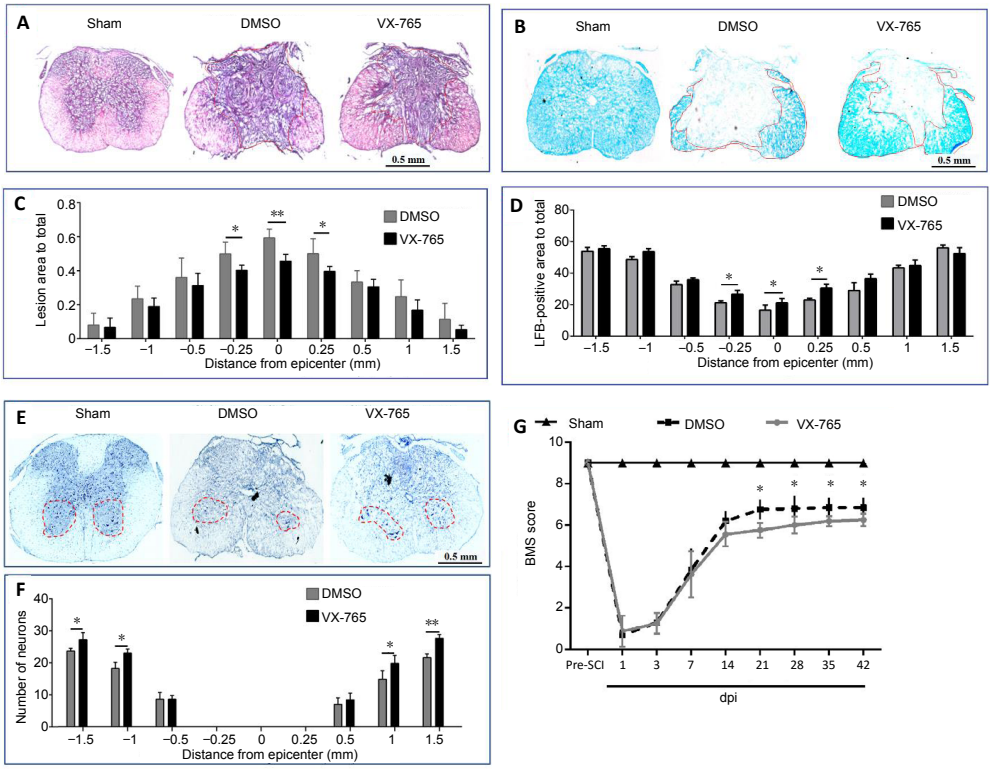

Figure 11 | Effects of VX-765 on histopathology and behavior after SCI at 42 days post-injury.
(A, B) Hematoxylin-eosin (A) and Luxol fast blue (B) staining in the injury epicenter. In hematoxylin-eosin-stained sections (A), the color of the fibrotic area was notably darker than in other areas. There was no fibrotic area in the sham-injured spinal cord. There were marked fibrotic areas in the injured spinal cords, and the fibrotic area of the VX-765 group was smaller than that of the DMSO group. For Luxol fast blue staining (B), blue represents myelinated areas. Although the myelinated areas decreased markedly after SCI, the myelinated area of the VX-765 group was larger than that of the DMSO group. (C, D) Quantitative analysis of the fibrotic area (C) and residual myelination (D). (E) Nissl-stained cross-section, 0.5 mm rostral to the epicenter. Although Nissl-stained neurons were observed in all groups, the number of neurons decreased markedly after SCI, and the neurons were increased in the VX-765 group compared with the DMSO group. Scale bars: 0.5 mm. (F) Quantitative analysis of the residual ventral horn motoneurons. (G) BMS scores. All data are represented as the mean ± SD (n = 10). The original data for Figure 11C, D, F, and G are shown in Additional file 11. *P < 0.05, **P < 0.01 (repeated measures two-way analysis of variance followed by Bonferroni's *post hoc* analysis). BMS: Basso Mouse Scale; DMSO: dimethyl sulfoxide; dpi: day(s) post-injury; SCI: spinal cord injury; VX-765: caspase-1 selective inhibitor.

Open peer reviewer: *Sidharth Mehan, Indo Soviet Friendship College of Pharmacy, India.*

Additional files:
Additional Table 1: *Information of antibodies used in immunohistofluorescence.*
Additional Table 2: *Information of antibodies used in flow cytometry.*
Additional file 1: *Open peer review report 1.*
Additional file 2: *Original data of Figure 2.*
Additional file 3: *Original data of Figure 3.*
Additional file 4: *Original data of Figure 4.*

Additional file 5: *Original data of Figure 5.*
Additional file 6: *Original data of Figure 6.*
Additional file 7: *Original data of Figure 7.*
Additional file 8: *Original data of Figure 8.*
Additional file 9: *Original data of Figure 9.*
Additional file 10: *Original data of Figure 10.*
Additional file 11: *Original data of Figure 11.*

References

Aceves M, Terminel MN, Okoreeh A, Aceves AR, Gong YM, Polanco A, Sohrabji F, Hook MA (2019) Morphine increases macrophages at the lesion site following spinal cord injury: Protective effects of minocycline. Brain Behav Immun 79:125-138.

Adornetto A, Russo R, Parisi V (2019) Neuroinflammation as a target for glaucoma therapy. Neural Regen Res 14:391-394.

Ahmed A, Patil AA, Agrawal DK (2018) Immunobiology of spinal cord injuries and potential therapeutic approaches. Mol Cell Biochem 441:181-189.

Ahuja CS, Nori S, Tetreault L, Wilson J, Kwon B, Harrop J, Choi D, Fehlings MG (2017) Traumatic spinal cord injury-repair and regeneration. Neurosurgery 80:S9-S22.

Basso DM, Fisher LC, Anderson AJ, Jakeman LB, McTigue DM, Popovich PG (2006) Basso Mouse Scale for locomotion detects differences in recovery after spinal cord injury in five common mouse strains. J Neurotrauma 23:635-659.

Chai L, Lü JL, Hu JT, Hu HH, Xu QJ, Yu JW, Quan RF (2021) Signal pathway variation after induction of inflammatory response in rats with acute spinal cord injury. Zhongguo Zuzhi Gongcheng Yanjiu 25:1218-1223.

Chen AC, Tran HB, Xi Y, Yerkovich ST, Baines KJ, Pizzutto SJ, Carroll M, Robertson AAB, Cooper MA, Schroder K, Simpson JL, Gibson PG, Hodge G, Masters IB, Buntain HM, Petsky HL, Prime SJ, Chang AB, Hodge S, Upham JW (2018) Multiple inflammasomes may regulate the interleukin-1-driven inflammation in protracted bacterial bronchitis. ERJ Open Res 4:00130-02017.

Chen J, Chen YQ, Wang SN, Duan FX, Shi YJ, Ding SQ, Hu JG, Lü HZ (2020a) Effect of VX-765 on the transcriptome profile of mice spinal cords with acute injury. Mol Med Rep 22:33-42.

Chen S, Yao L, Huang P, He Q, Guan H, Luo Y, Zou Z, Wei S, Peng G, Yan J, Chen R, Zhang Q, Tao A (2019) Blockade of the NLRP3/Caspase-1 axis ameliorates airway neutrophilic inflammation in a toluene diisocyanate-induced murine asthma model. Toxicol Sci 170:462-475.

Chen YJ, Zhu H, Zhang N, Shen L, Wang R, Zhou JS, Hu JG, Lü HZ (2015) Temporal kinetics of macrophage polarization in the injured rat spinal cord. J Neurosci Res 93:1526-1533.

Chen YQ, Wang SN, Shi YJ, Chen J, Ding SQ, Tang J, Shen L, Wang R, Ding H, Hu JG, Lü HZ (2020b) CRID3, a blocker of apoptosis associated speck like protein containing a card, ameliorates murine spinal cord injury by improving local immune microenvironment. J Neuroinflammation 17:255.

Christgen S, Place DE, Kanneganti TD (2020) Toward targeting inflammasomes: insights into their regulation and activation. Cell Res 30:315-327.

Fehlings MG, Wilson JR, Tetreault LA, Aarabi B, Anderson P, Arnold PM, Brodke DS, Burns AS, Chiba K, Dettori JR, Furlan JC, Hawryluk G, Holly LT, Howley S, Jeji T, Kalsi-Ryan S, Kotter M, Kurpad S, Kwon BK, Marino RJ, et al. (2017) A clinical practice guideline for the management of patients with acute spinal cord injury: Recommendations on the use of methylprednisolone sodium succinate. Global Spine J 7:203s-211s.

Flores J, Noël A, Foveau B, Beauchet O, LeBlanc AC (2020) Pre-symptomatic Caspase-1 inhibitor delays cognitive decline in a mouse model of Alzheimer disease and aging. Nat Commun 11:4571.

Flores J, Noël A, Foveau B, Lynham J, Lecrux C, LeBlanc AC (2018) Caspase-1 inhibition alleviates cognitive impairment and neuropathology in an Alzheimer's disease mouse model. Nat Commun 9:3916.

Fu KY, Tan YH, Sung B, Mao J (2009) Peripheral formalin injection induces unique spinal cord microglial phenotypic changes. Neurosci Lett 449:234-239.

Galanopoulou AS, Mowrey WB, Liu W, Li Q, Shandra O, Moshé SL (2017) Preclinical screening for treatments for infantile spasms in the multiple hit rat model of infantile spasms: An update. Neurochem Res 42:1949-1961.

Gosselin A, Monteiro P, Chomont N, Diaz-Griffero F, Said EA, Fonseca S, Wacleche V, El-Far M, Boulassel MR, Routy JP, Sekaly RP, Ancuta P (2010) Peripheral blood CCR4+CCR6+ and CXCR3+CCR6+CD4+ T cells are highly permissive to HIV-1 infection. J Immunol 184:1604-1616.

Greaves DR, Gordon S (2002) Macrophage-specific gene expression: current paradigms and future challenges. Int J Hematol 76:6-15.

Hayta E, Elden H (2018) Acute spinal cord injury: A review of pathophysiology and potential of non-steroidal anti-inflammatory drugs for pharmacological intervention. J Chem Neuroanat 87:25-31.

Hermiston ML, Xu Z, Weiss A (2003) CD45: a critical regulator of signaling thresholds in immune cells. Annu Rev Immunol 21:107-137.

Horiuchi H, Oshima Y, Ogata T, Morino T, Matsuda S, Miura H, Imamura T (2015) Evaluation of injured axons using two-photon excited fluorescence microscopy after spinal cord contusion injury in YFP-H line mice. Int J Mol Sci 16:15785-15799.

Hu JG, Shen L, Wang R, Wang QY, Zhang C, Xi J, Ma SF, Zhou JS, Lü HZ (2012) Effects of Olig2-overexpressing neural stem cells and myelin basic protein-activated T cells on recovery from spinal cord injury. Neurotherapeutics 9:422-445.

Hu JG, Shi LL, Chen YJ, Xie XM, Zhang N, Zhu AY, Jiang ZS, Feng YF, Zhang C, Xi J, Lü HZ (2016a) Differential effects of myelin basic protein-activated Th1 and Th2 cells on the local immune microenvironment of injured spinal cord. Exp Neurol 277:190-201.

Hu X, Liu X, Moisan J, Wang Y, Lesch CA, Spooner C, Morgan RW, Zawidzka EM, Mertz D, Bousley D, Majchrzak K, Kryczek I, Taylor C, Van Huis C, Skalitzky D, Hurd A, Aicher TD, Toogood PL, Glick GD, Paulos CM, et al. (2016b) Synthetic RORγ agonists regulate multiple pathways to enhance antitumor immunity. Oncoimmunology 5:e1254854.

Idriss HT, Naismith JH (2000) TNF alpha and the TNF receptor superfamily: structure-function relationship(s). Microsc Res Tech 50:184-195.

Jamilloux Y, Martinon F (2016) Cell-free assay for inflammasome activation. Methods Mol Biol 1417:207-215.

Karimi-Abdolrezaee S, Eftekharpour E, Wang J, Morshead CM, Fehlings MG (2006) Delayed transplantation of adult neural precursor cells promotes remyelination and functional neurological recovery after spinal cord injury. J Neurosci 26:3377-3389.

Karsy M, Hawryluk G (2019) Modern medical management of spinal cord injury. Curr Neurol Neurosci Rep 19:65.

Kawahara Y, Kaneko T, Yoshinaga Y, Arita Y, Nakamura K, Koga C, Yoshimura A, Sakagami R (2020) Effects of sulfonylureas on periodontopathic bacteria-induced inflammation. J Dent Res 99:830-838.

Kitamura K, Nagoshi N, Tsuji O, Matsumoto M, Okano H, Nakamura M (2019) Application of hepatocyte growth factor for acute spinal cord injury: The road from basic studies to human treatment. Int J Mol Sci 20:1054.

Latz E, Xiao TS, Stutz A (2013) Activation and regulation of the inflammasomes. Nat Rev Immunol 13:397-411.

Li Q, Dai Z, Cao Y, Wang L (2019) Caspase-1 inhibition mediates neuroprotection in experimental stroke by polarizing M2 microglia/macrophage and suppressing NF-κB activation. Biochem Biophys Res Commun 513:479-485.

Li Y, Niu X, Xu H, Li Q, Meng L, He M, Zhang J, Zhang Z, Zhang Z (2020) VX-765 attenuates atherosclerosis in ApoE deficient mice by modulating VSMCs pyroptosis. Exp Cell Res 389:111847.

Lin YH, Wu Y, Wang Y, Yao ZF, Tang J, Wang R, Shen L, Ding SQ, Hu JG, Lü HZ (2018) Spatio-temporal expression of Hexokinase-3 in the injured female rat spinal cords. Neurochem Int 113:23-33.

Liu S, Xie YY, Wang B (2019a) Role and prospects of regenerative biomaterials in the repair of spinal cord injury. Neural Regen Res 14:1352-1363.

Liu Z, Yang Y, He L, Pang M, Luo C, Liu B, Rong L (2019b) High-dose methylprednisolone for acute traumatic spinal cord injury: A meta-analysis. Neurology 93:e841-850.

Ma SF, Chen YJ, Zhang JX, Shen L, Wang R, Zhou JS, Hu JG, Lü HZ (2015) Adoptive transfer of M2 macrophages promotes locomotor recovery in adult rats after spinal cord injury. Brain Behav Immun 45:157-170.

Marchesan JT, Girnary MS, Moss K, Monaghan ET, Egnatz GJ, Jiao Y, Zhang S, Beck J, Swanson KV (2020) Role of inflammasomes in the pathogenesis of periodontal disease and therapeutics. Periodontol 2000 82:93-114.

Maroso M, Balosso S, Ravizza T, Iori V, Wright CI, French J, Vezzani A (2011) Interleukin-1β biosynthesis inhibition reduces acute seizures and drug resistant chronic epileptic activity in mice. Neurotherapeutics 8:304-315.

Martin E, El-Behi M, Fontaine B, Delarasse C (2017) Analysis of microglia and monocyte-derived macrophages from the central nervous system by flow cytometry. J Vis Exp:55781.

Martinon F, Burns K, Tschopp J (2002) The inflammasome: a molecular platform triggering activation of inflammatory caspases and processing of proIL-beta. Mol Cell 10:417-426.

McKenzie BA, Mamik MK, Saito LB, Boghozian R, Monaco MC, Major EO, Lu JQ, Branton WG, Power C (2018) Caspase-1 inhibition prevents glial inflammasome activation and pyroptosis in models of multiple sclerosis. Proc Natl Acad Sci U S A 115:E6065-6074.

Miyara M, Yoshioka Y, Kitoh A, Shima T, Wing K, Niwa A, Parizot C, Taflin C, Heike T, Valeyre D, Mathian A, Nakahata T, Yamaguchi T, Nomura T, Ono M, Amoura Z, Gorochov G, Sakaguchi S (2009) Functional delineation and differentiation dynamics of human CD4+ T cells expressing the FoxP3 transcription factor. Immunity 30:899-911.

Mortezaee K, Khanlarkhani N, Beyer C, Zendedel A (2018) Inflammasome: Its role in traumatic brain and spinal cord injury. J Cell Physiol 233:5160-5169.

Nikitina IY, Panteleev AV, Kosmiadi GA, Serdyuk YV, Nenasheva TA, Nikolaev AA, Gorelova LA, Radaeva TV, Kiseleva YY, Bozhenko VK, Lyadova IV (2018) Th1, Th17, and Th1Th17 lymphocytes during tuberculosis: Th1 lymphocytes predominate and appear as low-differentiated CXCR3(+)CCR6(+) cells in the blood and highly differentiated CXCR3(+/-)CCR6(-) cells in the lungs. J Immunol 200:2090-2103.

Noe FM, Polascheck N, Frigerio F, Bankstahl M, Ravizza T, Marchini S, Beltrame L, Banderó CR, Löscher W, Vezzani A (2013) Pharmacological blockade of IL-1β/IL-1 receptor type 1 axis during epileptogenesis provides neuroprotection in two rat models of temporal lobe epilepsy. Neurobiol Dis 59:183-193.

Popovich PG (2014) Neuroimmunology of traumatic spinal cord injury: a brief history and overview. Exp Neurol 258:1-4.

Porter AG, Jänicke RU (1999) Emerging roles of caspase-3 in apoptosis. Cell Death Differ 6:99-104.

Rose-John S (2018) Interleukin-6 family cytokines. Cold Spring Harb Perspect Biol 10:a028415.

Rouanet C, Reges D, Rocha E, Gagliardi V, Silva GS (2017) Traumatic spinal cord injury: current concepts and treatment update. Arq Neuropsiquiatr 75:387-393.

Rubiano AM, Carney N, Chesnut R, Puyana JC (2015) Global neurotrauma research challenges and opportunities. Nature 527:S193-197.

Sedgwick JD, Ford AL, Foulcher E, Airriess R (1998) Central nervous system microglial cell activation and proliferation follows direct interaction with tissue-infiltrating T cell blasts. J Immunol 160:5320-5330.

Sharma D, Kanneganti TD (2016) The cell biology of inflammasomes: Mechanisms of inflammasome activation and regulation. J Cell Biol 213:617-629.

Singh A, Tetreault L, Kalsi-Ryan S, Nouri A, Fehlings MG (2014) Global prevalence and incidence of traumatic spinal cord injury. Clin Epidemiol 6:309-331.

Stack JH, Beaumont K, Larsen PD, Straley KS, Henkel GW, Randle JC, Hoffman HM (2005) IL-converting enzyme/caspase-1 inhibitor VX-765 blocks the hypersensitive response to an inflammatory stimulus in monocytes from familial cold autoinflammatory syndrome patients. J Immunol 175:2630-2634.

Sun X, Jones ZB, Chen XM, Zhou L, So KF, Ren Y (2016) Multiple organ dysfunction and systemic inflammation after spinal cord injury: a complex relationship. J Neuroinflammation 13:260.

Teng YD, Mocchetti I, Wrathall JR (1998) Basic and acidic fibroblast growth factors protect spinal motor neurones in vivo after experimental spinal cord injury. Eur J Neurosci 10:798-802.

Thomas ML (1989) The leukocyte common antigen family. Annu Rev Immunol 7:339-369.

Thompson CD, Zurko JC, Hanna BF, Hellenbrand DJ, Hanna A (2013) The therapeutic role of interleukin-10 after spinal cord injury. J Neurotrauma 30:1311-1324.

Wannamaker W, Davies R, Namchuk M, Pollard J, Ford P, Ku G, Decker C, Charifson P, Weber P, Germann UA, Kuida K, Randle JC (2007) (S)-1-((S)-2-{[1-(4-amino-3-chloro-phenyl)-methanoyl]-amino}-3,3-dimethyl-butanoyl)-pyrrolidine-2-carboxylic acid ((2R,3S)-2-ethoxy-5-oxo-tetrahydro-furan-3-yl)-amide (VX-765), an orally available selective interleukin (IL)-converting enzyme/caspase-1 inhibitor, exhibits potent anti-inflammatory activities by inhibiting the release of IL-1beta and IL-18. J Pharmacol Exp Ther 321:509-516.

Wu J, Zhao Z, Kumar A, Lipinski MM, Loane DJ, Stoica BA, Faden AI (2016) Endoplasmic reticulum stress and disrupted neurogenesis in the brain are associated with cognitive impairment and depressive-like behavior after spinal cord injury. J Neurotrauma 33:1919-1935.

Wu Y, Lin YH, Shi LL, Yao ZF, Xie XM, Jiang ZS, Tang J, Hu JG, Lü HZ (2017) Temporal kinetics of CD8(+) CD28(+) and CD8(+) CD28(-) T lymphocytes in the injured rat spinal cord. J Neurosci Res 95:1666-1676.

Wu Y, Shen L, Wang R, Tang J, Ding SQ, Wang SN, Guo XY, Hu JG, Lü HZ (2018) Increased ceruloplasmin expression caused by infiltrated leukocytes, activated microglia, and astrocytes in injured female rat spinal cords. J Neurosci Res 96:1265-1276.

Yang XM, Downey JM, Cohen MV, Housley NA, Alvarez DF, Audia JP (2017) The highly selective caspase-1 inhibitor VX-765 provides additive protection against myocardial infarction in rat hearts when combined with a platelet inhibitor. J Cardiovasc Pharmacol Ther 22:574-578.

Yu N, Li X, Song W, Li D, Yu D, Zeng X, Li M, Leng X, Li X (2012) CD4(+)CD25 (+) CD127 (low/-) T cells: a more specific Treg population in human peripheral blood. Inflammation 35:1773-1780.

Zhang Y, Zheng Y (2016) Effects and mechanisms of potent caspase-1 inhibitor VX765 treatment on collagen-induced arthritis in mice. Clin Exp Rheumatol 34:111-118.

Zhang Y, Zhang Y, Gu W, Sun B (2014) TH1/TH2 cell differentiation and molecular signals. Adv Exp Med Biol 841:15-44.

P-Reviewer: Mehan S; C-Editor: Zhao M; S-Editors: Yu J, Li CH; L-Editors: Gardner B, Yu J, Song LP; T-Editor: Jia Y

Additional Table 1 Information of antibodies used in immunohistofluorescence

Antigen	Host species and clone	Cat# or Lot#	RRID	Source	Used concentration
CD11b	Rat monoclonal	14-0112-82	AB_467108	Invitrogen	1:200
CD45		14-0451-82	AB_467251		
CD68		MA5-16674	AB_2538168		
FOXP3		14-4776-82	AB_467554		
CD4		14-9766-82	AB_2573008		
CD4	Rabbit polyclonal	PA5-87425	AB_2804136		
GATA3		PA5-20892	AB_11154392		
T-bet		PA5-40573	AB_2576589		
RORγ (t)		PA5-23148	AB_2540675		
Arg1		PA5-29645	AB_2547120		
CCR7		ab191575		Abcam	
Rat IgG (H+L)	Fluorescein-conjugated goat polyclonal	112-095-143	AB_2338199	Jackson ImmunoResearch	
Rabbit IgG (H+L)	Rhodamine-conjugated goat polyclonal	111-025-144	AB_2337932		

Arg1: Arginase-1; CCR7: chemokine (C-C motif) receptor 7; FOXP3: forkhead box P3; GATA3: GATA binding protein 3; RORγ (t): retinoid-related orphan nuclear receptor γ-t; T-bet: Th1-specific T box transcription factor.

Additional Table 2 Information of antibodies used in flow cytometry

Antigen	Host species and clone	Cat# or Lot#	RRID	Conjugation	Source	Used concentration
CCR7	Rat monoclonal	47-1971-82	AB_2573974	AF780	Invitrogen	0.25 μg/test
IgG2bκ isotype control	Rat	47-4321-82	AB_1271997			0.25 μg/test
CD11b	Rat monoclonal	12-0112-81	AB_465546	PE		0.125 μg/test
CD3	Rat monoclonal	12-0032-82	AB_2811741			0.25 μg/test
IgG2bκ isotype control	Rat	12-4031-82	AB_470042			0.25 μg/test
CD127	Rat monoclonal	48-1273-82	AB_2574039	eFlour 450		0.5 μg/test
IgG2b κ isotype control	Rat	48-4031-82	AB_1272017			0.5 μg/test
CD183	Armenian hamster monoclonal	62-1831-82	AB_2762747	Super Bright 436		0.5 μg/test
IgG isotype control	Armenian hamster	62-4888-82	AB_2717007			0.5 μg/test
CD196	Rat monoclonal	50-7196-82	AB_11219682	eFlour 660		0.5 μg/test
IgG2a κ isotype control	Rat	50-4321-82	AB_10598503			0.5 μg/test
CD25	Rat monoclonal	47-0251-82	AB_1272179	AF780		0.5 μg/test
IgG1 κ Isotype Control	Rat	47-4301-80	AB_1271986			0.5 μg/test
CD28	Syrian hamster Monoclonal	45-0281-80	AB_925744	PerCP-Cyanine5.5		0.5 μg/test
IgG isotype control	Armenian hamster	45-4888-80	AB_906260			0.5 μg/test
CD3	Armenian hamster monoclonal	47-0031-82	AB_11149861	AF780		0.5 μg/test
IgG Isotype Control	Armenian hamster	47-4888-80	AB_1271978			0.5 μg/test
CD4	Rat monoclonal	11-0041-82	AB_464892	FITC		0.25 μg/test
CD68	Rat monoclonal	MA5-16676	AB_2538170			0.25 μg/test
IgG2bκ isotype control	Rat	11-4031-82	AB_470004			0.25 μg/test
CD45	Rat monoclonal	17-0451-82	AB_469392	APC		0.125 μg/test
IgG2b κ Isotype Control	Rat	17-4031-82	AB_470176			0.125 μg/test

AF780: APC-eFluor 780; APC: allophycocyanin; CCR7: chemokine (C-C motif) receptor 7; FITC: fluoresceine isothiocyanate; PE: phycoerythrin.

Quantitative results of microglia and infiltrated macrophages in injured spinal cord

		$CD45^+$ cells/mm^2	
	Sham	SCI(DMSO)	SCI(VX-765)
	20	627	906
	25	1186	1004
	35	1517	1087
	11	1243	865
	12	1114	1074
	17	1135	1032
mean	20	1137	994.6666667
SD	8.988882022	289.3682775	90.52660751

		$CD68^+$ cells/mm^2	
	Sham	SCI(DMSO)	SCI(VX-765)
	5	658	593
	7	872	596
	8	779	702
	11	676	619
	15	879	648
	16	814	701
mean	10.33333333	779.6666667	643.1666667
SD	4.457203907	94.99614027	49.30483411

		$CD11b^+$ cells/mm^2	
	Sham	SCI(DMSO)	SCI(VX-765)
	188	517	902
	185	1186	970
	175	1627	981
	171	1243	875
	172	1114	964
	211	1135	932
mean	183.6666667	1137	937.3333333
SD	15.09525312	357.3989368	42.06502902

		$CD68^+CD11b^+$ cells/mm^2	
	Sham	SCI(DMSO)	SCI(VX-765)
	0	708	615
	0	810	682
	0	802	664
	0	885	689
	0	776	674
	0	836	623
mean	0	802.8333333	657.8333333
SD	0	59.35795369	31.31400113

		$CD45^+CD11b^+$ cells/mm^2	
	Sham	SCI(DMSO)	SCI(VX-765)
	0	808	695
	0	764	672
	0	738	720
	0	848	695
	0	788	712
	0	807	703
mean	0	792.1666667	699.5
SD	0	38.29577871	16.64632091

Microglia and infiltrated macrophages: a flow cytometry assay

		cell subsets (%)								
		CD68+	CD11b+	CD45+	CD68+CD11b+	CD45+CD11b+	CD45-/lowCD11b+	CD45+CD68+	CD45-/lowCD68+	CD45+CD68-CD11b-
		0.628	0.726	0.239	0.426	0.112	0.907	0.055	0.698	0.12
		0.313	1.08	0.353	0.35	0.152	0.84	0.182	0.645	0.13
		0.41	1.254	0.226	0.435	0.143	0.81	0.01	0.689	0.1
sham		0.51	1.387	0.212	0.51	0.149	1.03	0.02	0.663	0.12
		0.921	0.527	0.093	0.342	0.084	0.789	0.039	0.794	0.12
		0.645	1.58	0.12	0.44	0.148	0.92	0.025	0.746	0.11
	mean	0.571166667	1.092333333	0.2071667	0.417166667	0.131333333	0.882666667	0.055166667	0.705833333	0.116666667
	SD	0.213274862	0.401182585	0.0930493	0.062764374	0.027449347	0.088957668	0.06408562	0.055257277	0.010327956

		CD68+	CD11b+	CD45+	CD68+CD11b+	CD45+CD11b+	CD45-/lowCD11b+	CD45+CD68+	CD45-/lowCD68+	CD45+CD68-CD11b-
		3.07	2.15	0.885	1.18	0.414	1.12	0.276	2.74	0.219
		2.092	1.96	0.834	0.572	0.318	0.787	0.282	1.9	0.274
		2.918	2.55	0.75	1.26	0.54	1.15	0.318	3.02	0.522
SCI(DMSO)		3.11	2.99	0.85	1.586	0.642	1.146	0.284	1.12	0.498
		3.31	3.17	0.72	1.476	0.416	0.9535	0.29	2.12	0.296
		2.412	2.56	0.701	1.512	0.418	1.157	0.302	1.7	0.374
	mean	2.818666667	2.563333333	0.79	1.264333333	0.458	1.05225	0.292	2.1	0.363833333
	SD	0.467491462	0.46586121	0.0761341	0.373113209	0.114437756	0.151007202	0.015491933	0.695240965	0.123910317

		CD68+	CD11b+	CD45+	CD68+CD11b+	CD45+CD11b+	CD45-/lowCD11b+	CD45+CD68+	CD45-/lowCD68+	CD45+CD68-CD11b-
		1.37	0.694	0.354	0.361	0.277	0.62	0.084	1.24	0.163
		1.86	0.85	0.652	0.331	0.383	0.893	0.091	1.35	0.21
		1.42	0.76	0.552	0.365	0.271	0.571	0.065	1.14	0.182
SCI(VX-765)		1.5	0.642	0.518	0.367	0.215	0.713	0.071	0.98	0.17
		1.62	1.02	0.491	0.358	0.325	0.792	0.04	1.11	0.189
		1.495	0.7925	0.525	0.355	0.221	0.706	0.072	1.05	0.176
	mean	1.544166667	0.793083333	0.5153333	0.356166667	0.282	0.715833333	0.0705	1.145	0.181666667
	SD	0.176420426	0.133018201	0.0966885	0.013090709	0.06388427	0.116150621	0.017694632	0.133078924	0.016573071

Quantitative results of M1 and M2 cells in injured spinal cord in injured spinal cord

	$CD68^{+}CCR7^{+}$ cells/mm^2		
	Sham	SCI(DMSO)	SCI(VX-765)
	22	625	564
	15	602	519
	23	673	497
	21	589	476
	13	803	569
	18	659	545
mean	18.66666667	658.5	528.3333333
SD	4.03319559	77.76310179	37.44685122

	$CD68^{+}Arg\text{-}1^{+}$ cells/mm^2		
	Sham	SCI(DMSO)	SCI(VX-765)
	36	165	245
	33	190	224
	28	212	240
	22	188	215
	32	172	218
	38	198	250
mean	31.5	187.5	232
SD	5.787918451	17.10847743	14.87279395

M1 and M2 Microglia/macrophages: a flow cytometry assay

cell subsets (%)

		CD11b+CD68+CCR7+	CD11b+CD68+CCR7-	CD45highCD11b+CD68+CCR7+	CD45highCD11b+CD68+CCR7-	CD45-/lowCD11b+CD68+CCR7+	CD45-/lowCD11b+CD68+CCR7-
		24.212	28.45	16.25	0	35.71	21.92
		31.75	32.12	23.28	0	34.35	26.12
		29.78	25.16	29.35	0	35.08	32.15
sham		28.97	31.412	24.11	0	32.01	25.55
		21.36	36.97	18.12	0	33.17	26.13
		30.13	38.88	28.22	0	35.02	28.68
	mean	27.70033333	32.16533333	23.22166667	0	34.22333333	26.75833333
	SD	4.015182271	5.130682866	5.252875086	0	1.385866756	3.418616192

		CD11b+CD68+CCR7+	CD11b+CD68+CCR7-	CD45highCD11b+CD68+CCR7+	CD45highCD11b+CD68+CCR7-	CD45-/lowCD11b+CD68+CCR7+	CD45-/lowCD11b+CD68+CCR7-
		57.18	13.23	67.23	0	65.26	5.79
		55.75	10.38	60.05	0	69.95	6.73
		59.38	13.59	52.16	0	73.26	7.54
SCI(DMSO)		51.71	8.06	53.47	0	72.39	6.21
		53.64	5.94	69.46	0	63.11	8.13
		56.98	14.36	58.11	0	71.32	6.12
	mean	55.77333333	10.92666667	60.08	0	69.215	6.753333333
	SD	2.738800224	3.393226586	7.062679378	0	4.106749323	0.909827823

		CD11b+CD68+CCR7+	CD11b+CD68+CCR7-	CD45highCD11b+CD68+CCR7+	CD45highCD11b+CD68+CCR7-	CD45-/lowCD11b+CD68+CCR7+	CD45-/lowCD11b+CD68+CCR7-
		37.32	20.88	37.02	0	57.58	10.41
		41.15	18.42	42.55	0	59.95	11.15
		45.36	22.36	49.42	0	63.81	13.79
SCI(VX-765)		49.51	10.86	39.98	0	57.11	10.22
		34.74	20.15	43.26	0	59.36	11.88
		39.22	14.22	37.54	0	58.97	9.37
	mean	41.21666667	17.815	41.62833333	0	59.46333333	11.13666667
	SD	5.423447858	4.408300126	4.580176489	0	2.386190828	1.554498847

Quantitative results of Th1, Th2 and Th17 cells in injured spinal cord in injured spinal cord

	$CD4^+T\text{-}bet^+$ cells/mm^2		
	Sham	SCI(DMSO)	SCI(VX-765)
	8	811	719
	2	797	705
	12	805	715
	10	754	685
	4	774	635
	15	816	702
mean	8.5	792.8333333	693.5
SD	4.888762625	24.06172618	31.02096066

	$CD4^+GATA3^+$ cells/mm^2		
	Sham	SCI(DMSO)	SCI(VX-765)
	5	133	285
	13	126	232
	5	123	175
	10	125	213
	12	138	263
	5	144	275
mean	8.333333333	131.5	240.5
SD	3.777124126	8.312640976	41.9416261

	$CD4^+ROR\gamma t^+$ cells/mm^2		
	Sham	SCI(DMSO)	SCI(VX-765)
	2	154	147
	6	167	175
	5	178	206
	3	166	173
	5	134	144
	4	189	172
mean	4.166666667	164.6666667	169.5
SD	1.471960144	19.13809465	22.52776065

Th1, Th2 and Th17 subsets: a flow cytometry assay

		cell subsets (%)			
		CD3+CD4+CD183+CD196-	CD3+CD4+CD183+CD196+	CD3+CD4+CD183-CD196+	CD3+CD4+CD183-CD196-
		0	0	0	0
		0	0	0	0
		0	0	0	0
sham		0	0	0	0
		0	0	0	0
		0	0	0	0
	mean	0	0	0	0
	SD	0	0	0	0
		CD3+CD4+CD183+CD196-	CD3+CD4+CD183+CD196+	CD3+CD4+CD183-CD196+	CD3+CD4+CD183-CD196-
		0	84.62	14.74	0.64
		4.6	84.05	11.03	0.32
		3.98	85.69	10.21	0.12
SCI(DMSO)		1	94.22	4.63	0.15
		4.56	83.24	11.84	0.36
		5.18	81.01	13.58	0.23
	mean	3.22	85.47166667	11.005	0.303333333
	SD	2.164070239	4.565397756	3.536986005	0.189384969
		CD3+CD4+CD183+CD196-	CD3+CD4+CD183+CD196+	CD3+CD4+CD183-CD196+	CD3+CD4+CD183-CD196-
		13.83	51.71	24.07	10.39
		7.44	74.06	13.35	5.15
		5.56	62.31	26.31	5.82
SCI(VX-765)		15.21	75.35	1.36	8.08
		5.57	68.97	20.05	5.41
		0	49.19	44.61	6.2
	mean	7.935	63.59833333	21.625	6.841666667
	SD	5.694203193	11.19817202	14.40738665	2.024405262

IHF quantitative results of Treg in injured spinal cord

		$CD4^+FoxP3^+$ cells/mm^2	
	Sham	SCI(DMSO)	SCI(VX-765)
	9	73	54
	5	54	64
	13	79	82
	10	78	67
	9	73	88
	8	59	56
mean	9	69.33333333	68.5
SD	2.607680962	10.36661308	13.7949266

FCM results of Treg in injured spinal cord

		Treg (%)	
	sham	SCI (DMSO)	SCI (VX-765)
	0	6.27	13.6
	0	11.3	21.2
	0	10.2	22.7
	0	6.78	15.2
	0	6.2	10.5
	0	4.5	12.56
mean	0	7.541666667	15.96
SD	0	2.624533609	4.907219172

IHF quantitative results of Tc in injured spinal cord

	$CD8^+CD28^+$ cells/mm^2		
	Sham	SCI(DMSO)	SCI(VX-765)
	13	367	238
	15	335	261
	22	386	221
	16	297	228
	28	318	257
	22	330	248
mean	19.33333333	338.8333333	242.1666667
SD	5.645056835	32.54176803	15.96767568

FCM quantitative results of Tc in injured spinal cord

	Tc (%)		
	sham	SCI (DMSO)	SCI (VX-765)
	0	97.6	96.7
	0	96.8	92.8
	0	97.8	96
	0	95.6	96.2
	0	93.7	94.5
	0	98.8	98
mean	0	96.71666667	95.7
SD	0	1.824737424	1.815488915

Quantitative results of histopathology and behavior

Lesion area to total

	Distance from epicenter	SCI(DMSO)						Mean	SD	SCI(VX-765)						Mean	SD
HE	-1.5	0.020934972	0.198672436	0.072790279	0.0421459	0.070142325	0.074313363	0.079833213	0.06194527	0.008040479	0.109652717	0.09122246	0.031848086	0.148935905	0.054825342	0.074087498	0.052303314
	-1	0.121614676	0.327233346	0.223957284	0.235502816	0.266272026	0.233989264	0.234761569	0.067028406	0.194124451	0.207606515	0.161656759	0.121239216	0.244912092	0.226950049	0.192748181	0.04515244
	-0.5	0.183455386	0.497416006	0.373046569	0.344640358	0.406002782	0.369580948	0.362357008	0.102598254	0.406444137	0.350279479	0.267345389	0.22573113	0.30295254	0.36252986	0.319213756	0.06654962
	-0.25	0.404871143	0.560123618	0.573021289	0.492982405	0.466293214	0.461224099	0.493085961	0.063872683	0.446932388	0.438074876	0.403895513	0.408224727	0.391682887	0.365713498	0.409087315	0.029948053
	0	0.566450781	0.667543714	0.624096417	0.543782021	0.567033142	0.575636801	0.590757146	0.04603607	0.520213838	0.514440653	0.462149192	0.429984932	0.452847603	0.417748096	0.466230719	0.042657856
	0.25	0.404532647	0.575882653	0.609305031	0.452777047	0.458449097	0.51087368	0.501970026	0.078576355	0.421355325	0.406510482	0.407645578	0.419734322	0.357829482	0.375977526	0.398175453	0.025619495
	0.5	0.235246608	0.383492388	0.405073129	0.310551853	0.334126376	0.401164851	0.344942534	0.065720063	0.363224541	0.294904199	0.243526245	0.29242032	0.319893854	0.30843719	0.303734391	0.039123711
	1	0.10300629	0.278985617	0.376672514	0.234993661	0.24298161	0.293184081	0.254970629	0.089982568	0.155089706	0.238256795	0.125708351	0.198799534	0.255819304	0.105663774	0.179889577	0.060974996
	1.5	0.036569092	0.154128774	0.259476982	0.077567317	0.040334827	0.06158069	0.104942947	0.08692401	0.017566131	0.087522688	0.067217507	0.039525132	0.085362316	0.05753885	0.059122104	0.027107653

LFB-postive area to total

	Distance from epicenter	SCI(DMSO)						Mean	SD	SCI(VX-765)						Mean	SD
LFB	-1.5	52.7	56.7	52.3	53.6	52.5	55.9	53.95	1.89076704	56.8	57.1	55.1	53.2	55	54.8	55.33333333	1.433410851
	-1	50.5	48.5	47.1	47.2	48.5	51.3	48.85	1.71784749	52.6	54.6	47.3	48.3	53.2	53.6	51.6	3.031171391
	-0.5	30.3	34.8	33.2	31.5	32.8	35.5	33.01666667	1.954908352	37.5	34.8	35.7	35.5	38.2	34.7	36.06666667	1.45143607
	-0.25	22.1	24	21.9	18.4	19.8	23.4	21.6	2.136352031	25.6	23.7	25.2	22.2	26.3	29.3	25.38333333	2.417781352
	0	13.3	16.7	19.7	11.6	15.7	20.1	16.18333333	3.392000393	19.2	20.3	24.1	19.2	21.7	18.6	20.51666667	2.070185177
	0.25	21.7	18.5	26.7	19.8	21.5	29.8	23	4.344191524	24.6	31.5	34.5	28.5	33.2	27.8	30.01666667	3.714521055
	0.5	31.4	20.3	31.3	31.5	30.8	33.7	29.83333333	4.778144689	36.9	35.4	33.4	34.5	35.3	29.5	34.16666667	2.559427019
	1	42.3	42.6	45.2	44.2	45.5	47.3	44.51666667	1.890414417	44.2	47.1	40.3	47.9	50.1	40.7	45.05	4.000874904
	1.5	57.4	56.8	54.1	56.2	54.1	57.3	55.98333333	1.519758753	48.3	50.5	54.4	56.6	55.2	51.2	52.7	3.18747549

Number of neurons

	Distance from epicenter	SCI(DMSO)						Mean	SD	SCI(VX-765)						Mean	SD
Niss	-1.5	23	27	23	25	23	20	24.2	2.34520788	31	26	27	26	26	27	27.16666667	1.940790217
	-1	18	24	19	19	15	15	19	3.326659987	25	20	22	23	23	23	22.66666667	1.632993162
	-0.5	7	12	7	9	8	9	8.6	1.861898673	10	8	9	9	7	8	8.5	1.048808848
	-0.25	0	0	0	0	0	0	0	0	0	0	0	0	0	0	0	0
	0	0	0	0	0	0	0	0	0	0	0	0	0	0	0	0	0
	0.25	0	0	0	0	0	0	0	0	0	0	0	0	0	0	0	0
	0.5	5	10	7	6	8	7	7.2	1.722401424	7	8	6	11	10	9	8.5	1.870828693
	1	10	20	12	12	15	18	13.8	3.885871846	18	24	19	18	20	20	19.83333333	2.228601953
	1.5	22	22	23	20	21	22	21.6	1.032795559	28	29	28	26	27	28	27.66666667	1.032795559

	Groups												mean	SD
BMS	sham	Pre-injury	9	9	9	9	9	9	9	9	9	9	9	0
		1 dpi	9	9	9	9	9	9	9	9	9	9	9	0
		3 dpi	9	9	9	9	9	9	9	9	9	9	9	0
		7 dpi	9	9	9	9	9	9	9	9	9	9	9	0
		14 dpi	9	9	9	9	9	9	9	9	9	9	9	0
		21 dpi	9	9	9	9	9	9	9	9	9	9	9	0
		28 dpi	9	9	9	9	9	9	9	9	9	9	9	0
		35 dpi	9	9	9	9	9	9	9	9	9	9	9	0
		42 dpi	9	9	9	9	9	9	9	9	9	9	9	0
	SCI(DMSO)	Pre-injury	9	9	9	9	9	9	9	9	9	9	9	0
		1 dpi	0.5	1.5	1.5	0	0.5	1	0.5	1.5	0	1	0.8	0.586893895
		3 dpi	1.5	1.5	1.5	0.5	1	1.5	1	2	0.5	1.5	1.25	0.485912658
		7 dpi	4.5	4	4	2	4	4.5	4	4.5	2	4	3.75	0.950146188
		14 dpi	5.5	6	6	4.75	5	6	5	6	4	5	5.325	0.687689368
		21 dpi	5.5	6.25	5.5	5.75	5.5	6.5	5	6.5	5	5.5	5.7	0.550252467
		28 dpi	5.5	6.5	6	6	6	6.5	5.5	6.5	5.5	6	6	0.40824829
		35 dpi	6	6.5	6.25	6	6	6.5	6	6.5	6	6	6.175	0.237170825
		42 dpi	6	6.5	6.5	6	6	6.5	6	6.5	6	6	6.2	0.25819889
	SCI(VX765)	Pre-injury	9	9	9	9	9	9	9	9	9	9	9	0
		1 dpi	0.5	1	0	1.5	0.5	0.5	1	1	0	1	0.7	0.483045892
		3 dpi	1	1.5	1.5	1.5	1	1	1.5	1.5	1.5	1.5	1.35	0.241522946
		7 dpi	3	3	5	4.75	3.5	4.5	4	5	4	4.5	4.125	0.756912589
		14 dpi	6	7	6	6	5.5	6	5.5	7	5.5	6	6.05	0.550252467
		21 dpi	6.5	7.5	6.5	7	6.5	6.5	6	7	6	6.5	6.6	0.459468292
		28 dpi	7	7.5	7	7	6.5	6.5	6	7	6	7	6.75	0.485912658
		35 dpi	7	7.5	7	7	7	7	6.5	7	6	7	6.9	0.394405319
		42 dpi	7	7.5	7	7	7	7	6.5	7	6	7	6.9	0.394405319